# POLITECNICO DI MILANO

School of Industrial and Information Engineering
Master of Science in Telecommunication Engineering


POLITECNICO
MILANO 1863

# A TUNING METHOD FOR PHOTONIC INTEGRATED CIRCUITS IN PRESENCE OF THERMAL CROSS-TALK


Supervisor: Prof. Andre Ivano MELLONI
Co.Supervisor: Dott. Ing. Francesco MORICHETTI
Ing. Maziyar MILANIZADEH

Candidate:
Sara AHMADI
Matr. n. 862555



Academic Year 2017/2018

Dedicated to my parents & Maman Aaki, Aghajoon
who raised me up and
supported me in every step
of my life.

# Abstract

Thermal Eigenmode Decomposition (TED) is introduced as a technique to cancel the effect of thermal cross-talk in photonic integrated circuits (PICs). This original technique, benefits from adopting eigen-solution of phase coupled system, allowing for an efficient tuning of the structure. This novel tuning scheme is exploited for a reconfigurable filter made of Mach-Zehnder interferometer (MZI) loaded by two Microring resonators (MRRs) and a mesh of MRRs.

Through numerical simulation and experimental tests, effectiveness of suggested technique is validated. For a MZI loaded by 2 MRRs, it is demonstrated that not only fine-tuned condition of the filter is achieved from random perturbations, but also the bandwidth is adapted to the channel spectrum. Via introduction of relevant goal functions, routing functionality in mesh of 4 MRRs, adopting the TED-based scheme is validated.
This method has the capability of extension to different photonic integrated circuits and platforms.

# Sommario

La decomposizione termica in autostati (TED) viene introdotta come tecnica per annullare l'effetto del cross-talk termico nei circuiti integrati fotonici (PIC). Questa tecnica originale sfrutta le autofunzioni dei sistemi accoppiati in fase, consentendo un' efficiente messa a punto della struttura. Questo nuovo schema di ottimizzazione é utilizzato per un filtro riconfigurabile costituito da un interferometro Mach-Zehnder (MZI) caricato con due risonatori ad anello (MRR) ed una mesh di MRR. Attraverso simulazioni numeriche e test sperimentali, é provata l'efficacia della tecnica suggerita. Per un MZI caricato con 2 MRR, non solo é dimostrato che é possibile ottenere un tuning fine del filtro per perturbazioni casuali, ma anche la larghezza di banda é adattata allo spettro del canale. Tramite l'introduzione di specifiche funzioni-obiettivo nello schema basato su TED viene verificata la funzionalit di routing in mesh di 4 MRR. Questo metodo ha la capacit di poter essere esteso a vari circuiti fotonici integrati, anche basati su diverse tecnologie.

# Contents

# List of Figures

# Chapter 1

# Control in integrated photonics

## 1.1 Introduction to integrated photonics

We live in a rapidly changing world where development in consumer technology are befalling so fast that the telecommunications network is struggling to keep up pace[18]. The fast uptake of smartphones/tablets and the widespread wireless streaming of high quality video and games are putting the conventional network architecture under immense pressure, and the problem is increasing as more applications are moving toward online infrastructure. Key examples include high definition 4K video streaming, the Internet of Things (IOT), the online health monitoring, cloud computing, and the trend of providing education completely online. Increase rates for data transmission vary across the telecommunication network depending on the source. However, it is widely known that yearly technological improvements in products placed within the network lag considerably behind the consumer demand. To keep pace with these rapid conversion, equipment manufacturers are expected to innovate more at scale, at speed and at cost. This highlights the importance of device and component integration to enable the next generations of efficient and scalable telecommunications products. The hight level of demanded integration has severe requirements for hardware design but even more considerable issues are arising from a thermal perspective. The thermal challenge increases with levels of integration, as the designer struggles to put more functionality into a smaller chip. Packing so much functionality (e.g., devices and components) into smaller package footprints will lead to substantial increase in thermal densities which in turn will require deployment of new thermal compensation solutions.

In the last years, photonic platforms with a high refractive index contrast have been attracting much interest, for the possibility to integrate many optical functions on a single chip. Among these, silicon-on-insulator (SOI) has emerged as a leading

technology for the compatibility with metal oxide semiconductor (CMOS) manufacturing, enabling the processing of large wafer sizes, high volume production and ultra-dense integration of extremely compact photonic circuits.

However, a significant challenge for high index contrast photonic platforms is associated to fabrication tolerance, highlighting the sensitivity of the effective index of the optical waveguides to nano-scale dimensional variations. These variations expose themselves in the form of phase errors in the photonic integrated devices. Considering that most photonic devices are based on interferometric-schemes , their behavior is altered immensely by any kind of phase perturbation. Furthermore, phase drifts may be also caused during the device operation by temperature variation.

To mitigate phase errors in photonic integrated circuits (PICs), actuators capable of actively controlling the phase shift in optical waveguides were deployed. As an example, thermal actuators, locally modifying the refractive index of the waveguide by thermo-optic effect, are a well-established method. However, thermal cross-talk effects between actuators controlling neighboring elements of the same photonic chip or among different circuits integrated onto the package may cause mutual unwanted phase perturbations and impair the control procedures.

## 1.2 Thermal cross-talk and necessity of control in integrated photonic

The ultimate goal of chip designer has always been the reduction of chip overall size. Moreover this trend is bond to increasing the chip functionality, yet holding the same fixed size as it is directly proportional to design and chip costs [26]. With the building block model, the approach of reducing the chip size is interpreted as reduction between distance of each components, since the functionality of each component (MMR, AWG, SOA ) is considered separately and optimized based on its own role. The main issue arises here in view of the fact that the minimum distance between building blocks cannot be easily manipulated since components interact with each other and this interaction become more severe as the distance decreases. This interaction between elements of a chip is commonly defined by the term, cross-talk [24]. Cross-talk is responsible for the maximum possible component density in a single chip. There are three kinds of cross-talk that contribute the most in photonic integrated circuits (PICs). These three forms are radio frequency cross-talk, which is related

to capacitive and inductive coupling of radio frequency signals, the optical cross-talk [101] addressed as light coupling between nearest elements and the scattered light; and thermal cross-talk, due to the transfer of gradient heat from active components like SOA, heaters, towards passive one, i.e. AWG, phase modulator, MRR and so on. Traditional consideration in electronics identify thermal control of the circuits for ensuring the long term operation of the system and so thermal management was consigned in the last steps of the design. But today thermal management stands as one of the biggest bottleneck for moving towards next generation of telecommunication equipment across entire network scaling from the nano (transistor/photonic active region) to the macro (datacenter/telecom network) range [19].

PICs are performing an ever increasing role in telecommunication and computing, but with respect to electronics they suffer more from temperature dependent performance. The thermal transfer over the chip poses drift in operational wavelength of the active and passive elements in the chip triggered by thermo-optical property of material and consequently led to degradation in signal to noise ratio (SNR) of the received signal and also bit error rate (BER). This problem become more critical regarding on-chip laser efficiency.

As an example a major challenge is present in tuning micro ring resonators (MRRs) [11]. The block of MRRs can be used for mux/demux operation, and they are extremely sensitive to refractive index changes. Thermal variation can shift a rings response off its designed resonant wavelength. Silicon-based ring resonators are specifically subjected to temperature-induced changes in refractive index (n) due to silicons large thermo-optic coefficient of $dn/dT = 1.86 \times 10^{-4}/K$. in [50] Resonance shifts of 0.1nm/K have been reported, which leads to considerable shift in wavelength caused by only few degrees of shift in temperature. Figure 1.1 depicts a WDM system consisting of MRR each including a local heater to tune their performance[11]. These temperature hot-spots will generate a thermal gradient over the chip. This thermal-induced change will push the rings to fall out of the designed resonance wavelength. And since the heat sources are local, each fragment of the chip is subjected to different temperature shift. Such thermal gradient put WDM networks based on ring resonator into significant operational challenge.

## 1.3 Control schemes in PICs

The issue related to thermal variation in on-chip optical communication has been addressed at both device and system levels[41]. At device level, solutions relying on

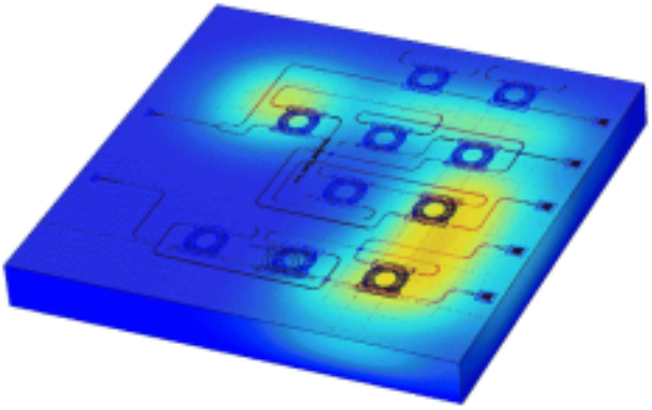

Figure 1.1: WDM system consisting of MRRs, each including a local heater to tune their performance

athermal-devices [15, 55], voltage tuning [51], local heating [6, 85], thermal-aware MR synthesis [12], and feed-back control schemes [95] have been explored to limit the thermal impact on or control the resonant wavelength of MRRs. At system level, the analyses allow the influence of temperature variation on the optical signal power received at receiver side [63, 94] to be evaluated.

Moreover, two general types of solutions has been offered to mitigate the vulnerability of index of refractive to temperature and fabrication imperfection. Part of these solutions are introduced based on tuning schemes to compensate for the problems, and the rest are a-prior permanent solutions aiming just to reduce the effect of thermal cross-talk inside the chip.

### 1.3.1 Passive tuning

Passive tuning is basically a permanent type of compensation that can be achieved by manipulating the optical properties of a waveguide's materials. There are some techniques in which exploit either geometry or modifies the structure's substances to meet the objection. One approach to circumvent these process variations is based on *Trimming* of the devices after fabrication. This is often performed by affecting the waveguides cladding layer through stress or additional material layers [81, 38].

In [25] another on-chip solution has been investigated to overcome the limit in miniaturization imposed by the thermal cross-talk. *Deep trenches* have been fabricated in Indium Phosphide (InP) platform by wet etching and used as solution to reduce the thermal cross-talk between active and passive components. The heat

sources are represented by semiconductor optical amplifiers placed at different distances with respect to the position of the Mach-Zehnder interferometers (MZI). Deep trench has been used as a means to modify the heat transfer path between optical components, since the air gap introduced through the aperture of the trenches act as the thermal isolator.

Another solution mentioned in [25] is to investigate based on *dry etch* of the InP to make the width and the depth of the trenches independent from each other. The best approach to isolate the passive components relies in etching completely the InP around them. So introducing deep rectangular shaped trenches could be considered as an step to reduce thermal cross-talk.

Another technique to reduce thermal effect is based on fabricating a *dummy silicon optical amplifier (SOA)* close to the main SOA to maintain a constant sum of the injected current in both SOAs. The effect is based on having the temperature around the SOAs area constant. This approach does not improve the miniaturization of the PIC since the dummy SOA requires a specific chip area for its definition and moreover the dummy SOA dissipates power without adding functionality.

In [86] two types of *conductive shunts* are introduced to improve the thermal dissipation due to poor thermal conductivity of buried oxide layer $K_{SiO_2} = 1.3W/m/K$ on structure consisting of a pre-patterned silicon on insulator wafer and III-V quantum well active region. There exist a strong temperature gradient across the buried oxide layer that highlights this layer as a significant barrier for heat flowing out of the III-V and into the Si substrate.

The first type of conductive shunts, relies on thermal shunts, where the buried oxide and epi silicon layers are etched away and backfilled with high thermal conductivity material. As in [86] Poly-Si thermal shunt technology is chosen due to its relatively high thermal conductivity ($k = 34W/m/K$) and compatibility with CMOS manufacturing, by doing so a reduction in thermal impedance $Z_t$ from 41.5 to $33.5C/W$ is observed. The second technology relies on metal shunts to reduce the thermal impedance in micro disk hybrid lasers. In this approach a metal pad is placed in contact with the micro disk to channel the heat away. Au ($K_{Au} = 317W/m/K$) is used to fill up etched box trench and attaches at the resonator sidewall. Metal part extract the diffused heat and leads to temperature drop.

In [29] an approach to eliminate the temperature sensitivity of Mach-Zehnder (MZ) modulators is investigated by adjusting the thermo-optic effects of their interfering arms through their *waveguide width and length optimization*. The core idea is based on a principle that the guided mode encounter different effective index changes with

temperature $\delta n_{eff}/\delta T$ in the two arms of MZI, induced by different waveguide widths. By choosing the arm lengths carefully, the temperature sensitivity of one arm can be set to cancel that of the other arm, and overall temperature sensitivity can be brought down to almost zero.

In [71] *liquid crystals* are exploit for passive temperature stabilization of silicon photonic devices. Liquid crystals possess high negative thermo-optic coefficient and their refractive index decreases linearly as temperature rises in both the anisotropic and isotropic phase. In [71] the method is validated for a ring resonator with air cladding which experience 87.5 pm/C resonance shift. By using different liquid crystal, better performances regarding to temperature fluctuation is met.

All the introduced methods aiming to create thermally insensitive structures , are well contributing to reduction of thermal cross-talk and adverse effects of heat variation inside the integrated chip, but they compensate until a certain degree and cannot be used to fully counteract the thermal issue, and to act so, they should be accompanied by other techniques to perform in a adequate level.
Besides, such athermal design methods require additional materials and lithographic processes that increase the cost and complexity of fabrication.

Contemporary literature proposes active compensation techniques to constantly monitor and tune the chip and hence overcoming any abrupt undesired influence arising from ambient, surroundings of the circuit and inside the chip itself.

### 1.3.2 Active tuning

Active compensation (tuning) utilizes external effects to change the optical properties of materials. For example, in silicon on insulator (SOI) ring resonators, active tuning is usually implemented via microheaters [21] exploiting silicons relatively large thermo-optic coefficient. Tuning by carrier-injection also applies a DC bias to the ring. Since highly doped P and N regions are used to form a P-i-N junction around the ring, and free-carriers injected into (conversely, extracted from) the rings to cause carrier concentration induced refractive index changes [83, 73]. In all such active compensation methods, outside energy and feedback are required to prevent resonance wavelength drift and offset. For instance, in the cited demonstration [2], changes in the temperature of a microring modulator were inferred by monitoring the mean power of the microring-modulated signal using an off-chip photo detector. And as the control system, the bias current is varied to provide the necessary temperature

adjustment in the localized region of the microring modulator. In [9] the results of [2] is further exploit and it is shown that optoelectronic components that comprise the control system can be integrated onto a single device using CMOS-compatible processes and materials. An important part of the active tuning scheme is feedback control part. In the last few years a significant amount of work has been done on the feedback control and on the wavelength locking of photonic integrated circuit [65, 64, 100, 13, 97, 27, 56, 87, 102, 61]. Research efforts in this field have been mainly focused on the mitigation of temperature sensitivity of optical waveguides and circuits, on feedback locking and stabilization of passive and active devices. Fig.1.2 summarizes and compares the primary techniques that were developed for the active stabilization of MRRs in Si photonics.

| Ref. | Device | Detection | Actuation | Technique & controller | Electronics | Sensitivity to power fluctuation | Locking position on MRR peak |
|---|---|---|---|---|---|---|---|
| MIT [35] | CW adiabatic MRR | 100% off-chip InGaAs PIN-TIA | Thermal, low doped Si regions | Min/max search, TIA+LPF+AD+FPGA digital | External lab instrumentation | Yes | Min/max |
| Columbia [28,29] [36,37] | CW MRR, 10 Gbit/s MRR modulator | On-chip tap defect enhanced Si PD, external PD | Thermal, Ti/NiCr heater or external TEC | Dithering, both analog and digital implementation, integral controller | External lab instrumentation | No | Min/max |
| Oracle [30] | 10 Gbit/s MRR modulator | On-chip Ge 20% tap PD | Thermal, metal heater | Bang-bang, sigma-delta, digital | CMOS integrated | Yes | ? |
| HP [32] | MRR | On-chip tap PD | Thermal, metal heater | Sigma-delta | CMOS integrated | Yes | Min/max |
| Sandia [31] | 5 Gbit/s MRR modulator | Two integrated Ge PDs (10% tap, 50% tap) | Thermal, metal heater | balanced homodyne detection, integral | External lab instrumentation | No | ? |
| Politecnico di Milano [33] | MRR | CLIPP, integrated transparent, no tap PD | Thermal, NiCr heater | Dithering, integral | CMOS integrated ASIC | No | Min/max |

Figure 1.2: State-of-the-art of the wavelength locking schemes for Si photonic MRRs.

Actually, in Ref. [65, 64, 100, 13, 97, 27], [87, 102, 61] only wavelength locking approaches for single MRRs were developed. Some of these techniques were demonstrated on microring modulators [65, 64, 100, 13]. Since the feedback loop is much slower than the bit-rate, locking a device in presence of a modulated signal has no impact on the control scheme.

On the contrary, having to lock a specific device such as a MRR modulator might affect the design of the locking scheme, in the sense that a specific device such as a

modulator might have particular working point, such as for instance along the slope of the resonant peak.

### 1.3.3 Key elements for control in PICs

Going through conventional approaches for control some issues must be considered to comprehensively conceive the control concept and various aspect associated with it. In the following section, general substances required in a generic control schemes is defined.

- **Detection**: all the proposed techniques require to monitor the optical power in some point of the MRR. Either done through a tap photodetector, that can be either integrated on-chip [65] [100, 13, 97] [1] or external [64] [87, 102] . Choice of monitoring point is a key element in performance of locking. Drop port or through port of filter or even monitoring the intensity inside resonators can be options to deploy the monitor.

- **Actuation**: all the experimental demonstrations employ thermal actuators: in [65, 64, 100, 13, 97, 27], [102, 61] conventional metallic heaters are utilized (typically fabricated in nickel chromium or titanium nitride), in [87] low doped Si regions. Thermal actuators fabricated through metal heaters are the legacy solution to compensate for temperature variations, yet their electrical power consumption is typically on the 1-10 mW scale to achieve a $\pi$-shift, and exhibit a time response on the microsecond scale [56] [60]. While their speed does not represent an issue to counteract relatively slow effects such as temperature drifts, thermal cross-talk or high-power induced thermal variations, their power efficiency should be improved to target ultra-low power solutions. In integrated photonics, thermal cross-talk plays an important role in introduction of perturbations between devices. Even inner thermal cross-talk plays a very important role in stability of a device, for example between resonators of a coupled MRR. These cross-talks introduce phase coupling which introduces unwanted changes in resonances of MRR. Robustness against this issue is a critical characteristic in the realization of a locking algorithm.

[1] Integrated tap PD for Si photonics are typically realized in germanium (Ge) [100] [13] or through defect-enhanced Si waveguides [65].

- **Electronics**: regardless of the control algorithm, the detector or the actuator etc., any wavelength locking approach requires some electronic control unit to manage the feedback loop. Demonstrations [87],[13], [65, 64] [102, 61] (MIT,Sandia, Columbia) have used off-chip laboratory instrumentation; while interesting for first proof-of-concept experiments, no evidence of potential on-chip integration has been shown.
  Oracle [100], HP [97] and our group at Politecnico di Milano [27] have shown wavelength locking of MRRs using CMOS integrated ASICs, and therefore have implemented approaches that are directly exploitable for real and system-level applications. Electronics are preferred to be as fast as possible to reduce delays in control loop. Usage of an FPGA or DSP in cases were complex calculations are required, is vital.

- **Sensitivity to power fluctuations**: as highlighted by Figure 1.2, whether or not a locking scheme works in presence of power fluctuations is a fundamental issue for its exploitation in real applications. In other words, the question is whether the locking approach keeps working properly in case of a power variation due to the external environment, such as for instance on a fiber optic link.

- **Wavelength locking demonstration**: it is worth noticing that, while Fig. Figure 1.2 lists all the publications that have claimed a demonstration of wavelength locking, not all of them have shown a clear evidence of such achievement [97], [87].

## 1.4 Tuning and locking techniques

As far as the approach of locking is concerned, Columbia university [102, 61],[65, 64] and our group [27] used a technique that exploits dithering signals because it offers a feedback system extremely robust to power fluctuations.
Also Sandia has developed an implementation that is insensitive to power drifts [13], yet as it relies on balanced homodyne detection, it seems to be hardly applicable to a generic photonic component or circuit, rather is specific to the circuit configuration of Ref. [13]. Oracle [100] and HP [97] have developed implementations based on sigma-delta comparator or bang-bang controller, whereas MIT [87] relies on a max/min search; the main limit of these implementations [100], [97], [87] really seems to be the detrimental dependence on power fluctuations.

As far as the controller type is concerned, most of the state-of-the-art implementations [65, 64], [102, 61], [13], [27] have used an integral controller; in Ref. [100] a bang-bang controller has been used. Dithering techniques are preferred to be avoided due to their power hungry nature. Speed of convergence (in terms of required iterations to compensate a perturbation) and robustness against input power fluctuations are two important characteristics to differentiate a locking method from others.

As a result, automatic configuration and wavelength locking is achieved by using feedback loops that sense the rings resonance conditions and tune the rings accordingly until the desired resonance conditions, or equivalently the filter responses, are reached. Typically, while sensing is performed using photo detectors external [47, 62] or internal [57, 20] to the rings, separate thermal tuners are required for tuning [48, 42].

In [36] automatic tuning of a four-ring Vernier filter across a 36.7-nm wavelength range spanning the the whole C-band is demonstrated by use of in-resonator photoconductive heaters (IRPHs) to both sense and tune the resonance conditions of ring resonators. IRPHs have the capability of both sensing and tuning the resonance condition of a ring resonator simultaneously. The tuning algorithm works based on finding the desired resonance condition of the $n_{th}$ ring, denoted as $R_n$ , by normalizing the cavity intensity of $R_n$, by the cavity intensity of the $R_{n-1}$ . Thus only one ring is tuned at a time, and at the end of each tuning step, the exact $\Phi_{th,n}$ satisfying $\Phi_n = \Phi_{0,n} + \Phi_{th,n} = 2(mod2\pi)$ is found, where $\Phi_{0,n}$ is the initial round-trip phase of the nth ring, and $\Phi_{th,n}$ is the phase introduced by thermal tuning.

In this method, rings $R_n$ through $R_1$ are sequentially tuned, starting from $R_N$ . Figure 1.3 shows the step corresponding to tuning the nth ring, $R_n$. While tuning $R_n$ , $I_{PD,n}$ and $I_{PD,n-1}$ are measured and the following optimization function is computed:

$$f_{OPT,n}(\Phi_{th,n}) = \begin{cases} \frac{I_{PD,n}(\Phi_{th,n})}{I_{PD,n-1}(\Phi_{th,n})} . \frac{I_{n-1}}{I_n} & \text{for n} > 1 \\ \frac{I_{PD,n}(\Phi_{th,n})}{I_n} & \text{for n=1} \end{cases} \tag{1.1}$$

Here $I_n$ and $I_{n-1}$ are the theoretical calculated cavity intensities of $R_n$ and $R_{n1}$ at $\Lambda_{in}$, respectively, $\Phi_{th,n}$ , or equivalently $V_n$ , is set to the value that maximizes $f_{OPT,n}$ $(\Phi_{th,n})$. Maximizing $f_{OPT,n}$ $(\Phi_{th,n})$ guarantees that the ratio of cavity intensities in rings $R_n$ and $R_{n-1}$ , measured by $I_{PD,n}$ $/I_{PD,n-1}$ , matches the expected intensity ratio $I_n$ $/I_{n1}$ . This, in turn, ensures that Rn is resonant at $\lambda_{in}$. When n = 1, $f_{OPT,1}(\Phi_{th,1})$ reduces to maximizing the intensity in $R_1$ . In equation 1.1, $f_{OPT,n}, (\Phi_{th,n})$ is always maximized when $\Phi_n = 0(mod2\pi)$, regardless of the resonance condition of $R_{n1}$ . The

purpose of $I_{PD,n1}$ is to works as a normalization factor for $I_{PD,n}$ as the amount of light coupling into $R_n$ at any point during the tuning step will depend on the cavity intensity in $R_{n-1}$.

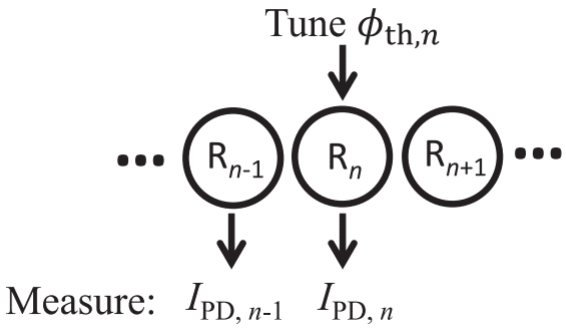


Figure 1.3: Tuning step for $R_n$, Photocurrents $I_{PD,n}$ and $I_{PD,n-1}$ are measured while tuning $\Phi_{th,n}$

It should be considered that applying such tuning to large scale PICs efficiently, requires considerable amount of time as current demonstrations of active feedback control for stabilization against thermal disturbances include many tuning steps, as each heater is tuned individually.

## 1.5 Thesis Contribution

In this work, we address the problem of controlling photonic integrated circuits in two different structures, including one chip of microring resonators (MRRs) and a Mach-Zehnder interferometer (MZI) chip loaded 2MRRs in the presence of thermal cross-talk by using a simple, yet efficient control algorithm.

All-pass MRRs combined with MZI allow a wide tunability range for the filter characteristics. Also MRRs itself, permit high level of integrations [45] as they provide a wide range of optical signal processing functions. For instance, they are used as building blocks in many architectures such as modulators [72], [96], amplifiers and lasers [74, 30, 31, 35, 89], wavelength converters [44] [79], switches and wavelength-division multiplexing (WDM) filters [78, 91, 39, 66, 92, 33]. In particular, photonic architectures based on coupled MRRs find many applications in optical signal processing and routing for optical communication and interconnect systems [43, 5, 90, 68]. To recover the desired passband, the resonances of the MRR could be aligned using phase actuators driven by suitable tuning strategies. However, for sophisticated structure to be suitable for volume production, control algorithms are required that enable resonance alignment not only in case of wide variability in the initial detuning but also when phase coupling effects between resonators occurs. If not considered, phase coupling may lead in fact to divergence in sequential tuning of resonators.

We develop a technique capable of tuning and locking filters in integrated optics exploiting thermo-optic phase shifters . This phase shifters are typically implemented using metallic [28] or doped-silicon [88] resistive heating elements that are widely used for tuning PICs. (Recently, germanium-based in-resonator photoconductive heaters have also been demonstrated for both sense and control operations [69], thereby avoiding the need for dedicated photodetectors. However, these devices required the deposition of germanium, increasing the complexity of fabrication.)

In our method, it is expected to compensate fabrication tolerances in the resonant wavelength regardless of temperature fluctuation due to environmental variation as well as thermal cross-talk effect from resonators of the same filter or other devices on the same chip. This technique must be able to maintain compensated filter status regardless of introduced perturbations. These perturbations can be in from of temperature, aging, signal wavelength or input power level variation. Compensation must be done transparent and without the need for a dedicated service time. Optimum monitoring point must be chosen for feedback purposes. This approach is expected to

account for phase coupling between resonators due the inevitable thermal cross-talk. Phase coupling introduce unwanted phase changes in the system.

## 1.6 Thesis Outline

The rest of thesis is organized as follows:

- Chapter 2 briefly defines the theory of microring resonators (MRRs) and their functionality, followed by mathematical description of the structure in different configuration used to model a simulator in MATLAB. Later on, the theory of Thermal Eigenmode Decomposition (TED) is defined, as an efficient algorithmic method to fine-tune the photonic integrated circuits.

- Chapter 3 is dedicated to experimental results of the introduce MRR structure. At the begging, the superiority of TED technique over other conventional methods, aiming to tune PIC is validated. Afterwards, a set of experiments are carried out to exploit the structure as a router.

- Chapter 4 attempts to implement the TED-technique on a new filter structure consists of MZI loaded by MRRs. Thereafter, the contribution of TED-algorithm on configuring and re-tuning the presented filter in presence of variation (thermal, input signal spectrum) is clarified.

- Finally Chapter 5 takes care of summary, conclusion and possible further extensions of the current work.

# Chapter 2

# Thermal Eigenmode Decomposition: theory and simulation

In this chapter, theoretical concepts related to microring resonators (MRRs) are introduced. It starts with a brief discussion over general properties of ring resonator, and expand it over to explore some typical existing configurations of MRRs.

Later on, the concept of **Thermal Eigenmode decomposition** (TED) is presented, as a technique to overcome thermal cross-talk effect. It is followed by establishing its advantages over other techniques, aimed to fine-tune the photonic integrated circuits in presence of thermal cross-talk.

Last part is dedicated to validating the possibility of fine-tuning a chip of MRRs via TED technique, through a numerical simulator in Matlab.
It would be of special interest to mention that TED is a general concept and has the capability of adaptation to any integrated structure. Indeed, at the beginning of study and to demonstrate a simple intuition to it, we exploit TED as a means to fine-tune a mesh of MRRs. The performance of this device is extremely sensitive to thermal variation, so it validates the TED-technique over a severe condition.

## 2.1 Microring resonators (MRRs)

Optical microring resonators (MRRs) are extensively described in literature [34, 82]. They attract too many application in telecommunication and also quantum computing systems as they offer high-order spectral features such as steep roll-offs and high extinction ratios. Generally, a ring resonator consists of a looped optical waveguide and a coupling mechanism to access the loop. Ring resonators can be studied as an interferometric device, that resonates for an input light with wavelength of multiple integer of rings circumference. When the waves inside the loop make a round trip phase shift that equals an integer times $2\pi$, the waves interfere constructively and places the cavity is in resonance condition.
In what follows, we briefly explain all concepts and formulas required to describe the functional behavior of ring resonators.

A basic arrangement of ring resonators labeled as All-pass configuration consists of unidirectional coupling between a ring resonator with radius $r$ and a bus waveguide is depicted in Figure 2.1

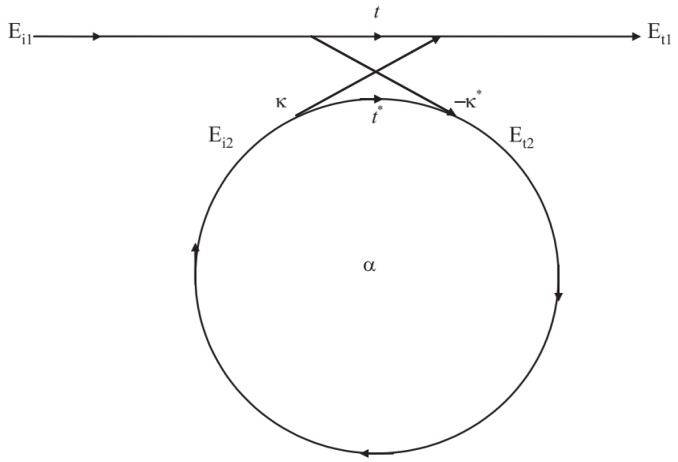


Figure 2.1: Model of single ring resonator with one bus waveguide[76]

The device in this configuration could be described as follow: Light source enters the device, via port $E_{il}$ and travels through the bus waveguide. The wavelength corresponding to resonant wavelength of the ring, is coupled to the ring, and the portion of the input light that is not corresponding to the resonance condition of the ring, will leave the structure through port $E_{t1}$ without any further effects on its intensity or phase.

Equation 2.1 aims to mathematically describe the resonance wavelength of a simple ring resonator.

$$\lambda_r = \frac{2\pi R n_{eff}}{m}. \tag{2.1}$$

Where $R$ is the ring radius constructed by a circular waveguide, $m$ is an integer and $n_{eff}$ is the effective refractive index of the structure. To further study and mathematically model the structure, the interaction of input, coupled and the output light with reference to Figure 2.1 is expressed in matrix below:

$$\begin{pmatrix} E_{t1} \\ E_{t2} \end{pmatrix} = \begin{pmatrix} \mathrm{t} & \mathrm{k} \\ -k^* & t^* \end{pmatrix} \begin{pmatrix} E_{i1} \\ E_{i2} \end{pmatrix}. \tag{2.2}$$

Where, $E$ is the normalized complex mode amplitude, $k$ and $t$ are the coupling parameters. Their values could differ based on the specific coupling mechanism used. Since the matrix is symmetric, we have: $|k^2| + |t^2| = 1$. In order to simplify the model we choose $E_{i1} = 1$. The round trip $E$ is then given by:

$$E_{i2} = \alpha e^{j\theta} E_{t2} \tag{2.3}$$

where $\alpha$ is the loss coefficient of the ring (zero loss: $\alpha = 1$) and $\theta = \omega L/c$, L being the circumference of the ring ($= 2\pi R$) and $c$ is light velocity inside the ring ($c = c_0/neff$), and finally $\omega$ is the angular frequency.
with further quantitative manipulation [75] these final equations are obtained for $E$ on the resonance condition:

$$E_{t1} = \frac{-\alpha + t.e^{-j\theta}}{-\alpha t^* + e^{-j\theta}} \tag{2.4}$$

$$E_{i2} = \frac{-\alpha k^*}{-\alpha t^* + e^{-j\theta}} \tag{2.5}$$

$$E_{t2} = \frac{-k^*}{1 - \alpha t^* e^{i\theta}} \tag{2.6}$$

and below corresponding values are obtained for power:

$$P_{t1} = |E_{t1}|^2 = \frac{(\alpha - |t|)^2}{(1 - \alpha|t|)^2} \tag{2.7}$$

$$P_{i2} = |E_{i2}|^2 = \frac{\alpha^2(1 - |t|^2)}{(1 - \alpha|t|)^2} \tag{2.8}$$

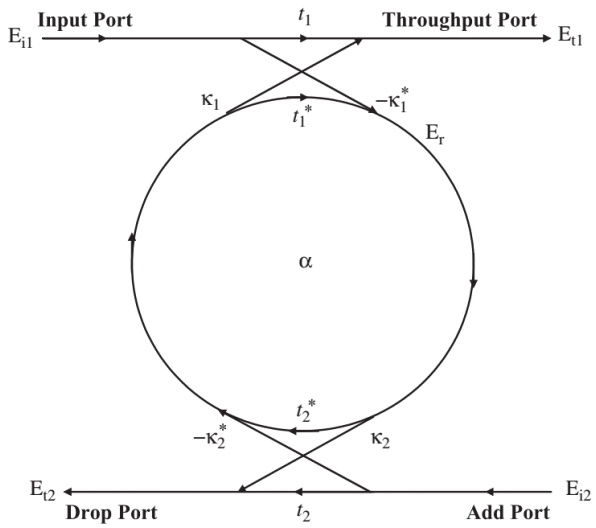


Figure 2.2: Model of ring resonator in add-drop configuration[76]

By means of these generic equations, it is possible to establish a rough idea on ring resonator's functionality.

The next structure is a ring resonator in add-drop configuration. This configuration has four ports referred as input, throughput(Through), drop and add port, as depicted in Figure 2.2.

Following equation describes power in the drop port:

$$P_{drop} = |E_{drop}|^2 = \frac{(1-|t_1|^2)(1-|t_2|^2).\alpha}{(1-\alpha|t_1 t_2|)^2} \tag{2.9}$$

In ring's resonance frequency the through port amplitude, $E_{t1}$, is equal to zero (for $t_1 = t_2$ and $\alpha = 1$). It indicates that in the resonance condition, power is completely extracted by the ring itself and eventually will exit through the drop port.

Figure 2.3 depicts two free spectral range (FSR) of through and drop ports' transfer function of MRR in add-drop configuration. As illustrated in the figure, in this configuration it is expected to experience a notch in resonant wavelength while monitoring the through port, as the whole power is resonating inside MRR itself.

The resonance wavelength of a ring resonator can be actively tuned in several ways, and thermal tuning is the most widely used technique. Thermal tuning exploits this to the effective index and thereby the spectral response, according to equation 2.1.

Figure 2.4 shows the drop spectrum and resonance wavelength shift of ring filter as a function of temperature, respectively. In practice, inside photonic chips, each element requires an individual heat source to address them separately. This is achieved

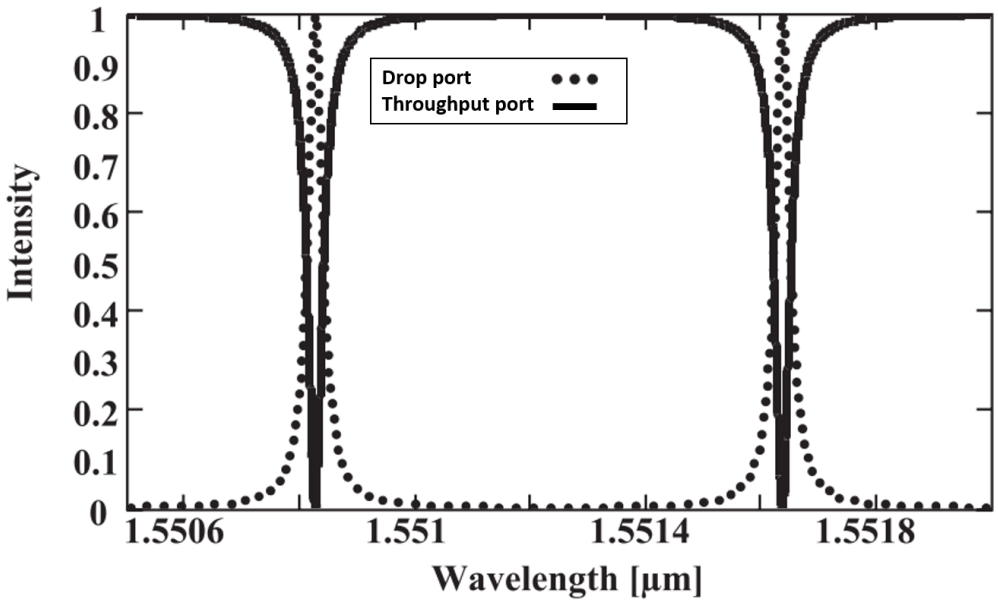


Figure 2.3: Transfer function of a MRR in add-drop configuration

by using micro-heaters, which can be placed either at the top or at the side of the device as a heat source with sufficient isolation to avoid optical loss. The most common heater configuration (which is also the case in our experimental chip) is placing the heater on top of the device [22, 17, 4, 23]. However, other configurations such as a lateral placement is available using CMOS process.

## 2.2 Thermal cross-talk model

For illustrating the concept of the thermal cross-talk, let us consider the schematic of Figure 2.5(a) showing an arbitrary photonic integrated circuit (PIC) consisting of $N$ optical waveguides with thermal actuator integrated in each of them. The status of circuit is identified by the phase vector $\Phi = [\Phi_1 ... \Phi_N]^T$, where $\Phi_n$ is the current phase in n-th waveguide. When an electrical power is applied to the n-th actuator, it is expected to introduce a desired phase change $\delta\Phi_n$ to the n-th waveguide, where the actuator is integrated, with no effect on the surrounding waveguides. However, due to thermal cross-talk, some phase perturbations are also introduced in the other waveguides. Considering Figure 2.5(a) the actual phase shifts $\delta\tilde{\Phi} = [\delta\tilde{\Phi}_1 ... \delta\tilde{\Phi}_N]^T$

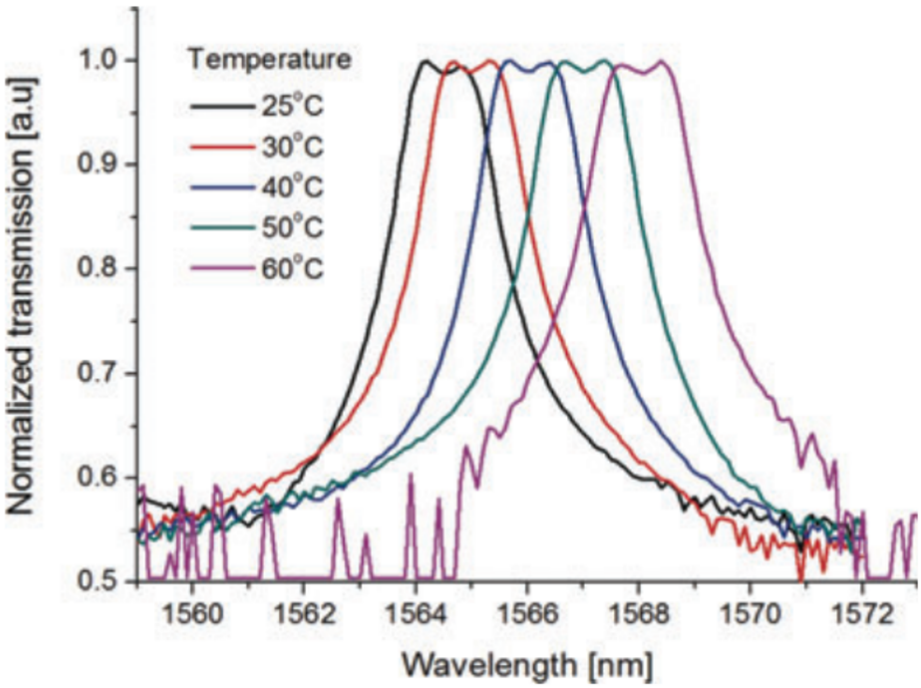


Figure 2.4: Shift of resonance wavelength in a generic 2nd order MRR versus temperature variation

induced in each waveguide is given by:

$$\delta\tilde{\Phi} = \begin{pmatrix} T_{11} & T_{12} & T_{13} & ... & T_{nn} \\ T_{21} & T_{22} & T_{23} & ... & T_{nn} \\ T_{31} & T_{32} & T_{33} & ... & T_{nn} \\ ... & ... & ... & ... & ... \\ T_{n1} & T_{n2} & T_{n3} & ... & T_{nn} \end{pmatrix} \delta\Phi = T\delta\Phi. \tag{2.10}$$

Where $\delta\Phi = [\delta\Phi_1 ... \delta\Phi_N]^T$ is the desired phase shift and $T$ is the phase coupling matrix taking into account all the self (diagonal) and cross (off-diagonal) phase shift contributions. Without loss of generality, all the diagonal terms can be assumed unitary, that is $T_{nn} = 1$. The phase coupling coefficient $T_{nm}$ between the n-th actuator and the m-th waveguide depends on the PIC topology, photonic platform and not the status of the circuit.

When applying control algorithms for the automatic tuning of the PIC, mutual phase perturbation among thermal actuators must be compensated. However, individual correction of each phase change $\delta\tilde{\Phi}_n$ is not an effective method for controlling the system. First, this would require for each actuator the need for post-compensating the thermal cross-talk that has been introduced by other actuators at previous steps,

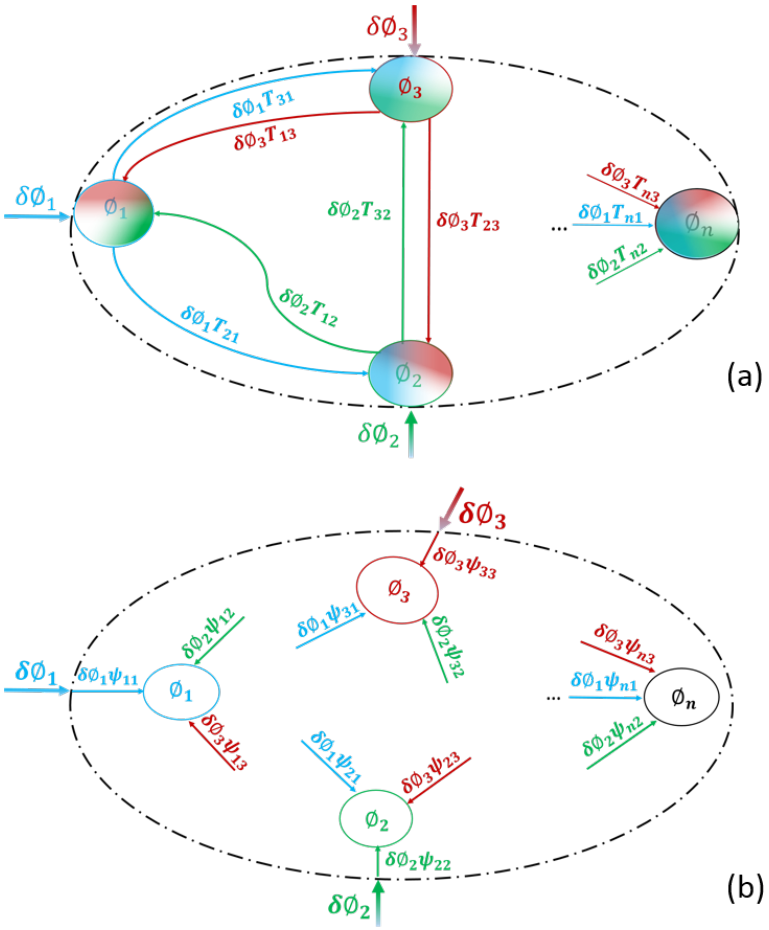


Figure 2.5: (a) Schematic representation of a PIC integrating N phase actuators in presence of phase coupling induced by thermal cross-talk. (b) TED concept: the effects of thermal cross-talk are canceled by simultaneously driving all the coupled actuators according to the eigenmodes of the thermally coupled system.

thus leading to a substantial increase of iteration number required to steer the PIC to the desired working point.

## 2.3 Introduction to Thermal Eigenmode Decomposition (TED)

To circumvent presented issue, we propose Thermal Eigenmode Decomposition (TED) method. TED provides a strategy to cancel out the unwanted effects of thermal cross-talk on the actual phase shift applied to the optical waveguide. Mathematically, the concept is extremely simple because it is essentially a coordinate transformation, mapping the phase variables $\Phi$ , which are thermally coupled by the $T$ matrix, into

a suitable set of uncoupled phase variables $\Psi = [\delta\Psi_1 ... \delta\Psi_N]^T$, for which the phase coupled matrix $T_D$ becomes diagonal. Assuming $T$ to be diagonalizable, we can write:

$$\delta\tilde{\Phi} = PT_DP^{-1}\delta\Phi. \tag{2.11}$$

Where $P$ is a matrix whose columns are linearly independent eigen-vectors of $T$, $T_D$ is the diagonal matrix containing the corresponding eigen-values, and $P^{-1}$ is the inverse matrix of $P$. Multiplying both side by $P^{-1}$ we obtain:

$$\delta\tilde{\Psi} = T_D\delta\Psi \tag{2.12}$$

where

$$\delta\Psi = P^{-1}\delta\Phi \tag{2.13}$$

is the phase shift imparted to the transformed phase variables $\Psi$. Since $T_D$ is diagonal, any change in each element of vector $\Psi$ does not effect the other elements. In other words, the elements $\Psi_n = P_n^{-1}\Phi$ where $P_n^{-1}$ is the n-th row of the $P^{-1}$ matrix, identify orthogonal directions in a transformed phase space, enabling to apply uncoupled, and hence well controllable, phase modification to the system.

From physical stand point, the TED method implies that all the actuators, that are thermally coupled, need to be simultaneously modified to apply the desired change. The wights are defined by the eigenmodes of the thermally coupled system, that is by the rows of the $P$ matrix.

To further illustrate the concept of thermal eigenmode decomposition, we use the structure of mesh of 4 MRRs depicted in the Figure 2.6 to practically establish the theory on.

The round trip phases of each MRR is shown in the figure ($\phi_i$ with $i = 1, 2, 3, 4$). we suppose that due to some perturbations, the phase of MRRs are drifted away with respect to objective tuning points. This phase shift is called $\delta\phi_i$ and it could be either positive or negative. To counteract this effect, a phase shift equal to $-\delta\phi_i$ should be applied to each MRR. As defined earlier, due to thermal cross talk phenomenon between heaters, also neighboring heaters will go through undesirable phase shift originated from correction voltage applied to each individual MRRs.

So considering the system consisted of 4 interconnected MRRs, if we apply the required amount of voltage to get the desired phase shift in each of them, the resulting transfer function would be nothing like the intended one as a result of unwanted

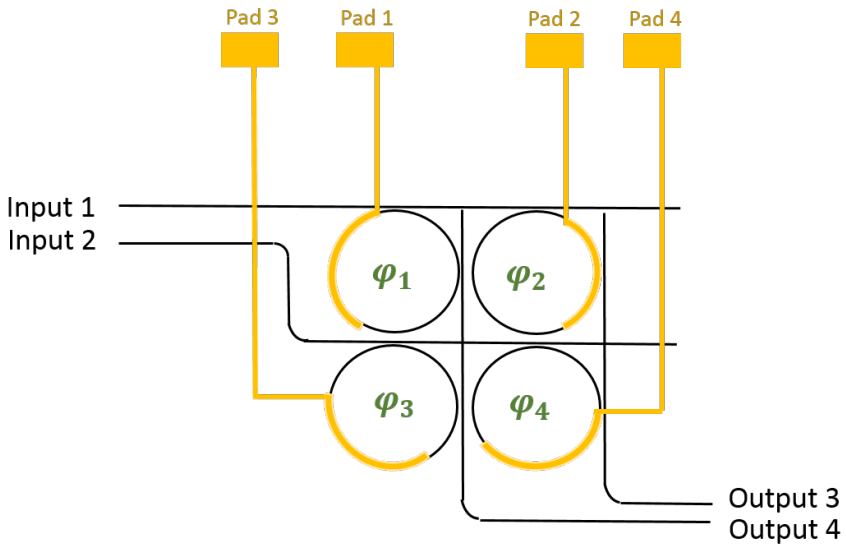


Figure 2.6: Mesh of interconnected MRRs

coupling arising from thermal cross talk phenomenon. The phase coupling matrix of the current structure is as follow:

$$\begin{pmatrix} \delta\tilde{\phi}_1 \\ \delta\tilde{\phi}_2 \\ \delta\tilde{\phi}_3 \\ \delta\tilde{\phi}_4 \end{pmatrix} = \begin{pmatrix} 1 & \mu & \mu & \mu \\ \mu & 1 & \mu & \mu \\ \mu & \mu & 1 & \mu \\ \mu & \mu & \mu & 1 \end{pmatrix} \begin{pmatrix} \delta\phi_1 \\ \delta\phi_2 \\ \delta\phi_3 \\ \delta\phi_4 \end{pmatrix}. \tag{2.14}$$

Where $\delta\phi_i$ are the intended applied phase shifts whilst "$\delta\tilde{\phi}_i$"s are the changes induced to each MRRs due to phase coupling phenomenon. For sake of simplicity we consider equal cross-talk between all heaters noted as $\mu$.

By extracting the eigenvectors of phase coupling matrix introduced in equation 2.14, a correct direction of movement is applied to heaters simultaneously, to counter effect the cross-talk in each step. below matrix is the eigenvector of the structure:

$$P = \begin{pmatrix} -1 & -1 & -1 & 1 \\ 1 & 0 & 0 & 1 \\ 0 & 1 & 0 & 1 \\ 0 & 0 & 1 & 1 \end{pmatrix}. \tag{2.15}$$

These orthogonal vectors promise an uncoupled compensations in a sense that steps taken in these direction would not perturb neighboring MRRs.

TED proposes $\psi_i$ vectors as the new coordinate to perform the control operation on. The values on matrix below define efficient weights of each component of new coordinate vector to be taken in each iteration:

$$\begin{pmatrix} \delta\psi_1 \\ \delta\psi_2 \\ \delta\psi_3 \\ \delta\psi_4 \end{pmatrix} = \begin{pmatrix} \frac{-1}{4} & \frac{3}{4} & \frac{-1}{4} & \frac{-1}{4} \\ \frac{-1}{4} & \frac{-1}{4} & \frac{3}{4} & \frac{-1}{4} \\ \frac{-1}{4} & \frac{-1}{4} & \frac{-1}{4} & \frac{3}{4} \\ \frac{1}{4} & \frac{1}{4} & \frac{1}{4} & \frac{1}{4} \end{pmatrix} \begin{pmatrix} \delta\phi_1 \\ \delta\phi_2 \\ \delta\phi_3 \\ \delta\phi_4 \end{pmatrix}. \tag{2.16}$$

## 2.4 Tuning and locking of MRRs: numerical modeling

After defining TED as a general technique capable of practicing different tasks, we exploit it for fine-tuning in integrated structures. In general, locking process exploit different measures as the reference signal. Our choice of reference goal is based on measured optical power.

The flowchart 2.7 is a generic chart summarizing the steps taken in tuning process. The reference signal at the objective point is measured, then it is compared with the goal point. The succeeding steps will be taken based on the distance of measured signal and the reference point. If the swept step, results in a poorer status with respect to prior measurement, the direction of movement is altered. To apply TED as a mean to lock the structure we proceed with the same flowchart but the steps are taken based on eigenvectors, and the corresponding round trip phase is calculated and applied. After each step, if the monitored power proceeds towards the desired value, same steps are taken, otherwise the direction of movement is reversed simply by changing the sign of $\delta\psi$. One output port is selected to monitor the power and the goal is to reach the maximum power.

The choice of stopping point for the algorithm depends on the implementation scenario. Best approach is knowing how close is the algorithm (filter shape) to the goal (shape of the fine-tued filter ) and choose the stopping point based on that. Percentage of power at defined port of the fine-tuned filter can be a stopping point. Locking method presented here is capable of real time implementation (meaning as a never ending process) but for the sake of simulation in this chapter a stopping point is always used to stop the iterations. Continuously taking steps in eigenvectors (change in

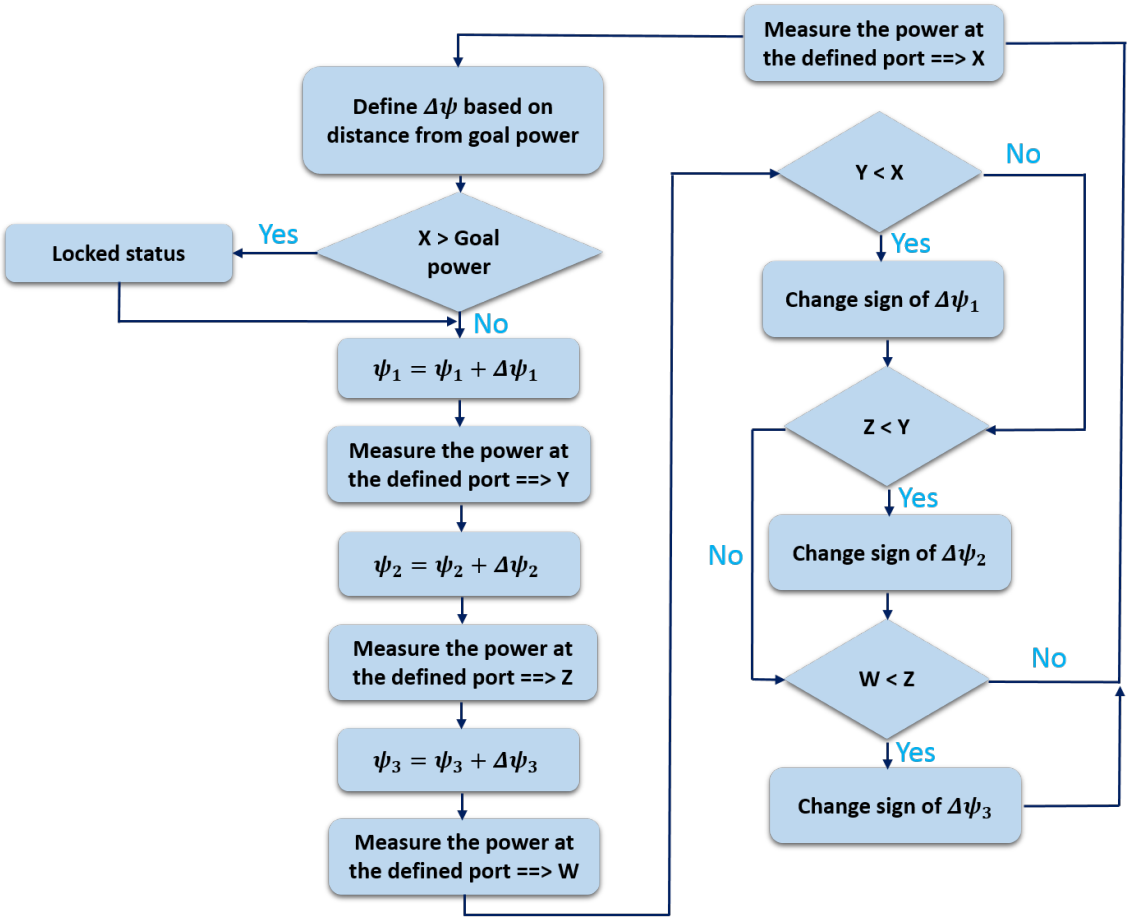


Figure 2.7: Flowchart of a generic tuning process

round trip phases of each ring) leads to possibility of observing external perturbations like temperature or wavelength drifts after reaching the fine-tuned filter. Relevant compensation can be applied to maintain this status of tuning. Consequently, there will be small residual oscillations in transfer function of locked filter. This oscillation can be minimized by decreasing the step size while being close to the optimum point. This could be practically done in adaptive stepping scheme, which step size evolve based on the distance of sampled signal from the preset goal point.

### 2.4.1 Simulation of routing input signal

The software package used to model the structure and the parameters associated with it is MATLAB R2017. for each chip, a mathematical model describing the functionality of circuit is developed inside MATLAB. Through and drop port transfer functions are calculated on defined number of frequency points. The frequency range in which the simulation is performed is defined based on the tuning range (in this case of analysis its one FSR of the filter which is about 50GHz) while considering minimum acceptable frequency resolution. Output power at drop or through port is calculated using optional input power (choice of modulation scheme and bit rate). This power is exploit in tuning and locking process. This numerical simulator can consider coupling noise, thermal cross talk between resonators to evaluate the efficiency of tuning methods in existence of these kinds of imperfections. It can introduce perturbations in form of input power variation, wavelength fluctuation to examine the locking methods.

Random initial cases of perturbed filter (by introducing a random shift in round trip phase of each ring) are introduced and round-trip phase of each MRR is swept searching for max optical power. In practice sweeping is done while taking steps in heater voltages but here for the sake of modeling, these steps are taken in round-trip phase of each MRR. The goal power to stop is defined based on maximum iteration number. However, it is possible to stop after reaching a certain percentage of power which outlines the multiplication of signal and filter in frequency domain. The frequency resolution in simulation is about 50MHz. The first simulation models the task of tuning and routing input signal to a desired output.

Among all the components that must be integrated into the network to allow on-chip photonic communication, switches are the fundamental building blocks capable of routing the signals along the different ports of the network thus connecting the different processors. In our case the switching mechanism corresponds to the signal path, depend on the variation of the refractive index induced by the applied voltage.

The switching velocity of the active device can significantly influence the overall network functionality as it contributes to signal delay.

We initiated 100 random cases to model diverse range of perturbed transfer function to lunch the algorithm on. As mentioned earlier, in real experiment these cases are modeled by random set of input voltages injected to heaters but here we introduce them as random round-trip phase inside each ring. With reference to Figure 2.6, we lunch the input spectrum from input port 2 and extract it from output port 3, so only MRRs 3 and 4 are involved in forming the final transfer function. We execute the feedback scheme by choice of maximizing the output power. In this argument, MRR 4 is expected to route the signal to its drop port which corresponds to the output port.

Figures 2.9 and 2.10 depict initial random perturbed filters and final locked and tuned filters, respectively.

Drop port of MRR4, functions as the filtering component to route the desired spectrum of input signal out. Therefore as expected, the round trip phase of MMR4 in all the cases have to converged to the same value, to maximally route the input signal towards its output port. It is well grounded that starting points are disregarded in study of locked filter, as they don't leave an impact on the final result.

These tests highlighted TED capability of locking and tuning integrated chip.

### 2.4.2 Comparison between individual-based and TED-based tuning

Up to know, the standard solutions for the tuning problem have been based on individual tuning of each element separately. As TED provides a transparent scheme for tuning and does this task in a orthogonal manner in which cross-talk effect is canceled automatically. We expect it yields significant speed advantage over conventional individual methods of tuning. To verify this property, we lunch a comparison test between TED-based and individual-based tuning method.

10 cases for initial perturbed filter are lunched identically for TED and individual tuning and the result in term of required iteration number in order to converge to the goal point is established.

Figure 2.8illustrates the final result. Blue-solid lines represent TED-based tuning and red-dashed lines are individual-based tuned. There is a clear advantage in following TED-technique for tuning the integrated chip in term of speed and also accuracy. As later will be discussed, individual-based tuning method not only speed down the tuning procedures but also fail to converge in some certain cases.

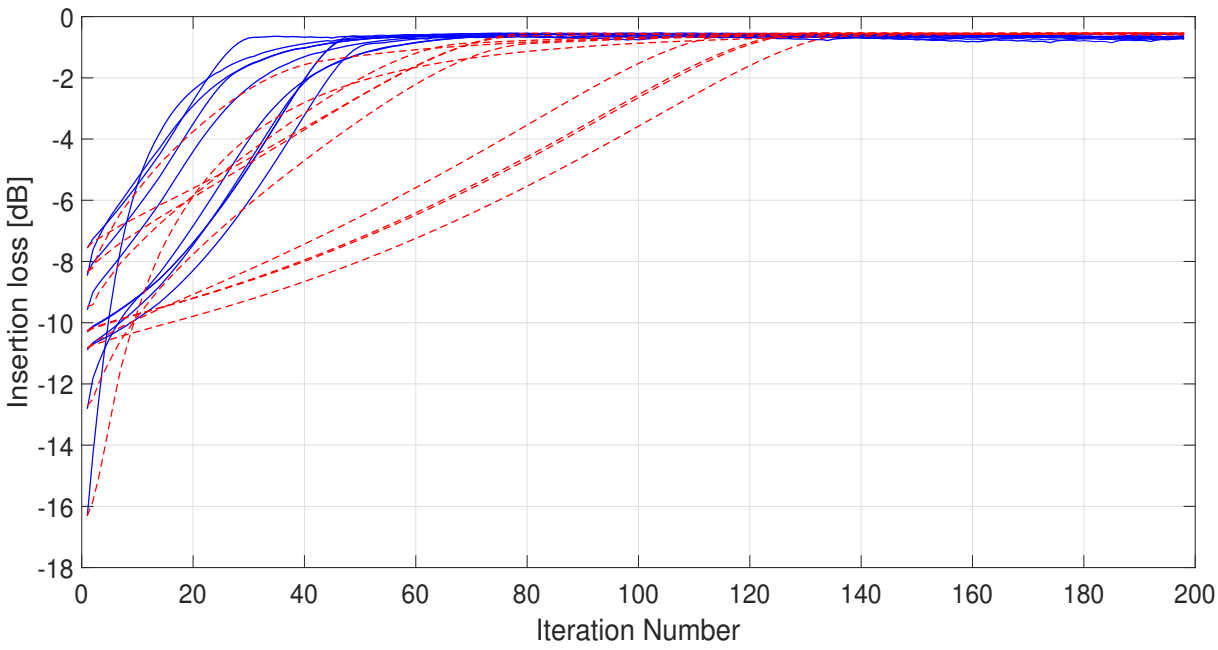


Figure 2.8: Power gradient change of individual and TED based tuned filters Blue curves are TED-based and red curves are corresponding results for individual-based tuning.

In the next chapter, further experimental tests are carried out to remark the peculiarity of TED-technique also in term of practical performance.

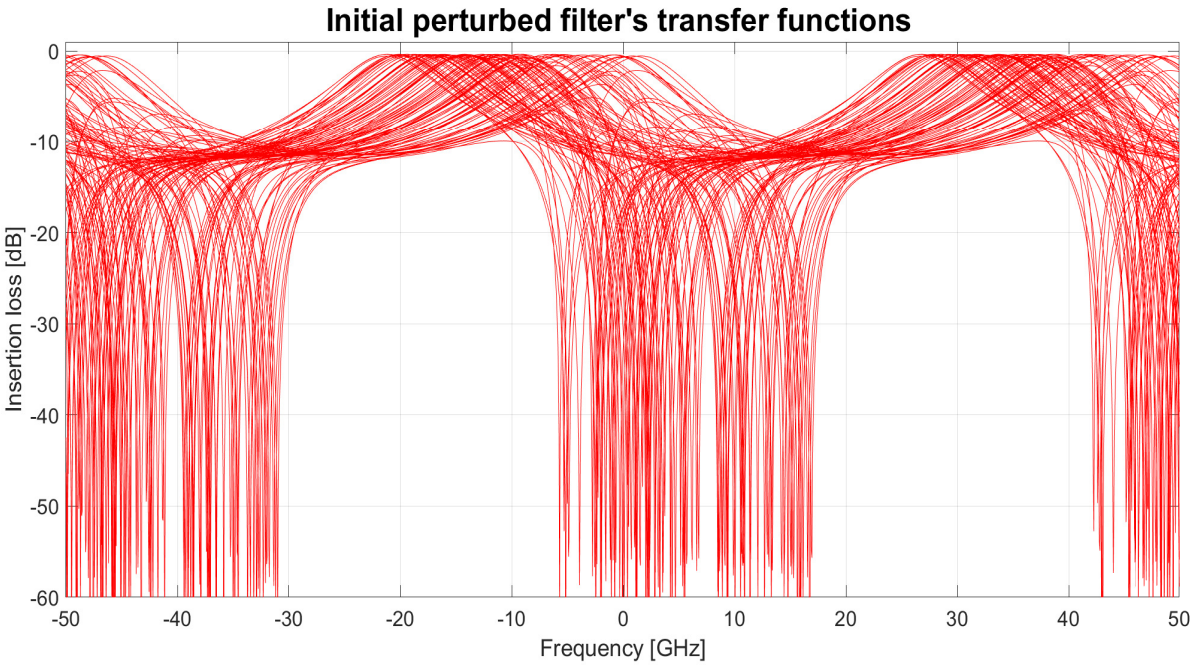


Figure 2.9: Initial random cases

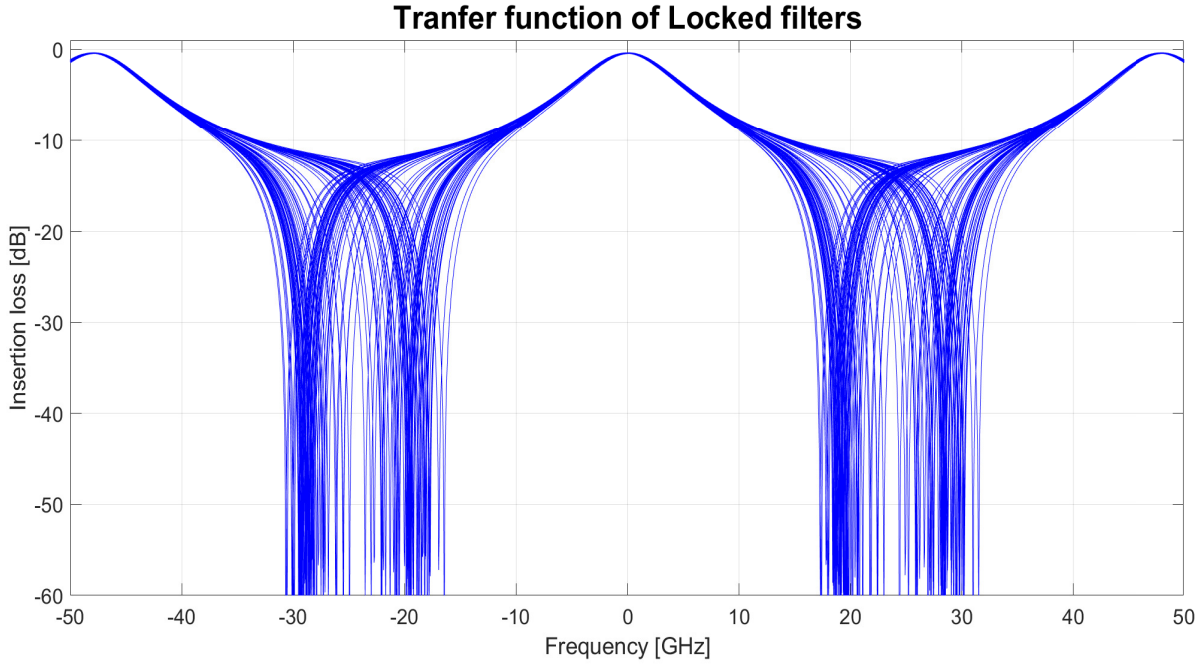


Figure 2.10: Transfer function of fine-tuned filters with TED technique

# Chapter 3

# Experimental results

This chapter is dedicated to practical experiments performed on mesh of Microring Resonators (MRRs).

It starts by introducing the fabrication technology of the chip under test, followed by defining the experimental setup.
The fabrication platform of the device under test (DUT) is in high-index-contrast Silicon Oxynitride (SiON). It is important to mention that although in this thesis TED is only applied on a certain photonic platform, it is a general algorithm and it can be implemented on different photonic fabrication technology as Silicon, Silicon on Insulator (SOI), Indium Phosphide (InP) and etc.

Later on, different scenarios are defined and experimentally evaluated, including ability of chip to follow the input signal by assistance of TED technique.

In the final part, the performance of structure is evaluated in absence of TEC controller (which fixes temperature of chip on a certain degree).

## 3.1 Silicon oxynitride (SiON) technology in integrated photonics

The technology used for fabricating the under test structure (mesh of 4 MRRs) is in high-index-contrast Silicon Oxynitride (SION) waveguides.[1] In this technology the optical waveguide has a square shape with almost $2.2 \times 2.2$ $\mu$m size.
A Scanning electron microscope (SEM) photograph of the waveguide cross section is reported in Figure 3.1(a), and in Figure 3.1(b) the coupling region of a directional coupler, before the deposition of the upper cladding, is illustrated.

The Sion core, with a refractive index $n_{Sion}$=1.513, is deposited by Plasma Enhanced Chemical Vapour Deposition (PECVD) on a thermal silicon dioxide substrate with $n_{Si02} = 1.4456$. The waveguide index-contrast is about 4.5%. Before lithographic processes, an annealing treatment at 1100 C has been conducted to reduce both material losses and stresses. A 200 nm under-etching was required to completely remove the SiON layer within the gap region of the couplers, where the etch rate is slower. As upper-cladding material, BP (Boron-Phosphorous) glass was employed rather than PECVD SiO2 because it was found to guarantee better performance in the waveguide coverage. Complete gap filling was observed in the gap region of directional couplers for distance between waveguides down to 1.6 $\mu$ m, corresponding to an aspect ratio of 1.4:1.

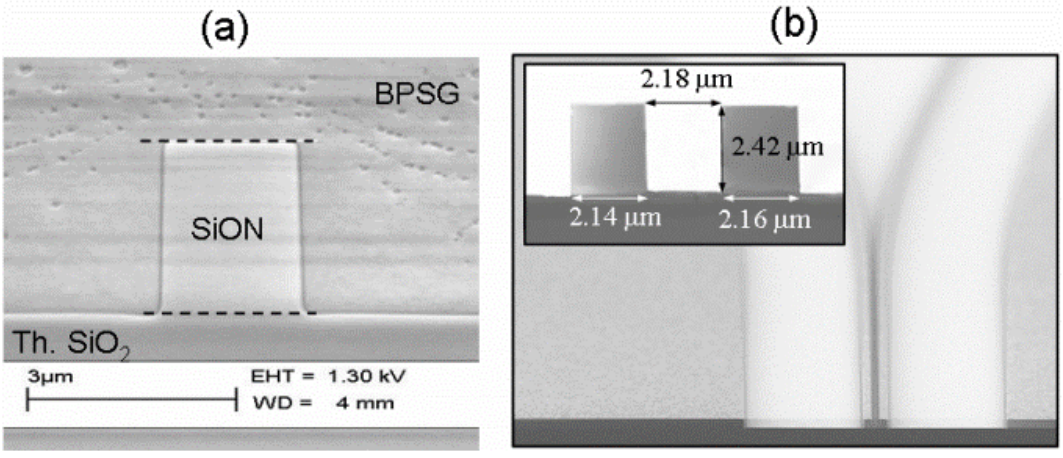


Figure 3.1: (a) SEM photograph of the SION buried waveguide cross-section; (b) top-view photograph of a directional coupler realized in SION technology. In the inset of the figure the waveguide cross section in the coupling region of the coupler is shown.

The filter is made from four interconnected MRRs as illustrated in Figure 3.6. Based on the specific use, we choose one of the topmost ports as input and rightmost ports as output. Evidently, by selecting different ports as input/output, different transfer functions are observed, as explained in previous chapter.
Depend on the function, we can opt for diminishing the undesired wavelengths by exiting within through port of a MRR which its resonance is set to that specified wavelength or leaving through drop port of a MRR to let the desired wavelength appears on the output.

## 3.2 Experimental setup

In this part, we go through all the details on the test setup. The described setup is used in all the experiments presented in this thesis. Any further details related to other sections will be pointed out if necessary. Schematic of the entire setup is depicted in Figure 3.2.
The setup consists of a electrical and a optical portions.

- **Optical section** Starting from left part of the figure, tunable laser source initiates the light signal followed by polarization controller in which sets the polarization of input light to match with modulator. Then the input light enters the modulator while the modulation scheme is customized for each experiment. In almost all the cases the modulation scheme is OOK except the one which is QPSK and will be point out in its order. Later on, an Erbium-doped fiber amplifier (EDFA) is exploit to compensate for excessive loss as EDFA is also amplifying spontaneous emission, it is followed by a tunable bandpass filter (BPF) with span of 2nm in charge of rejecting the off-band noise caused by EDFA. After BPF, another polarization controller is used to tune the existing status of light inside optical fiber to its optimum level to be launched into the chip, and since the embedded waveguides in Sion is sensitive to polarization status of input light, this task should be carried on carefully. Using variable optical attenuator, desired level of power is launched into chip through a small core fiber.
  At the output of the chip, series of dividers are used to split the optical power into 3 branches. One is supplied into optical spectrum analyzer (OSA) to observe and analyze the transfer function of filter. Second path is fed to a power meter for measuring the average optical power, this is used during the alignment of fibers/chip and also for manual observation of the power variation during the

locking process. The last branch is fed to a photo diode which is connected to signal acquisition system consisting of a Lock-in amplifier.

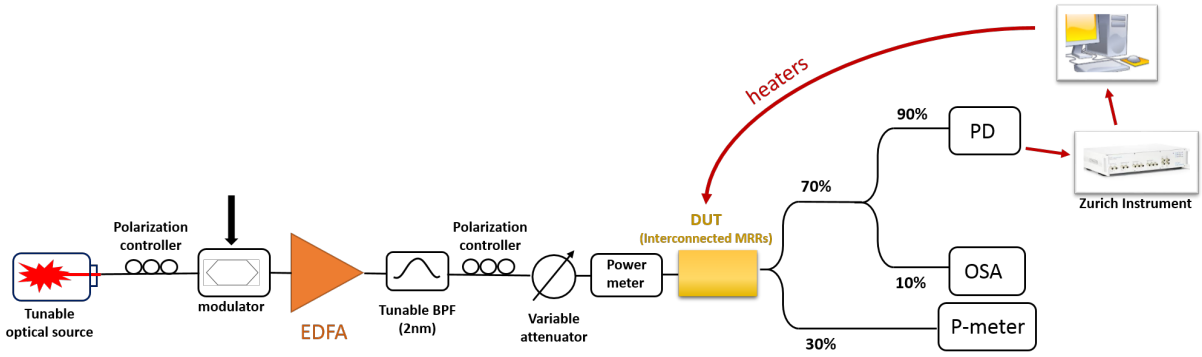


Figure 3.2: Schematic of entire test bench setup

- **Electrical section** The lock-in amplifier (Zurich Instruments HF2LI + MF + RT) has 6 independent Lock-In frequencies, 2 analog input (210 MSa/s, DC to 50MHz), 2 primary + 4 auxiliary outputs, 2 auxiliary inputs embedded microblaze processor for real-time operation. In the experiments 4 aux outputs and one aux input are used to control the filter. Zurich instrument is controlled by a PC through USB interface and provides 4 outputs to control the 4 heaters of the filter and one input to read the voltage of photo diode.

  Auxiliary outputs of Zurich are limited between +-10 volts which limits the dynamic range of heaters. To overcome this limitation a voltage source is used to provide a virtual ground for 4 outputs extending their voltage range as shown in Figure 3.3.

  By setting the external voltage source at +5 V the range is extended to 15 volt. Therefore in the represented experiments -5 volt at the output of Zurich Inst. corresponded to zero volt for heaters, like wise +10 means 15 volt applied to them. Overall current passing through the external source presents the total power fed to the chip and must be monitored during the locking not to exceed the burn out limit of heaters.

Picture of the bench is presented in Figure 3.4 And the top view of the chip is shown in Figure 3.5.

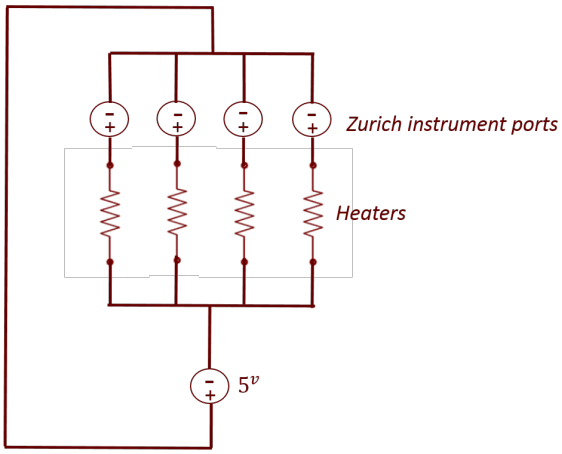


Figure 3.3: Circuit for extension of heaters' voltage dynamic range

The temperature of the chip is controlled by a thermoelectric cooler (TEC) which is controlled via closed loop controller. The feedback system is provided by a thermo-resistor attached to the holder. (temperature stability is in order of 0.01 degree and it is fixed at 25 degree).

Another significant part of electrical portion is the modulation board. The peculiarity of proposed experimental tuning scheme is presence of modulated signal as the input signal instead of continuous wave (CW) laser signal. Most of tuning methods have been tested via CW input signal [49]. Modulated signal offers a set of more accurate results for real application. Here, we benefit from both OOK and QPSK-modulated signals.

## 3.3 Experimental results on MRRs circuit

In this section, we illustrate the results of experiments performed in the integrated photonic laboratory. The chip under test is shown in Figure 3.6. As disclosed in the figure, it consists of mesh of 4 MRRs. The gold lines are metal conductive tracks connected to pads in one end, and heaters on other end, responsible for the current flowing into heaters. This current is controlled by voltage assessment on the pad and it is transformed to heat which modifies local refractive index of the material leading to change in MRRs' resonant wavelength.
There exist four input and four output ports. Either of them could be chosen based on the task required to be performed.

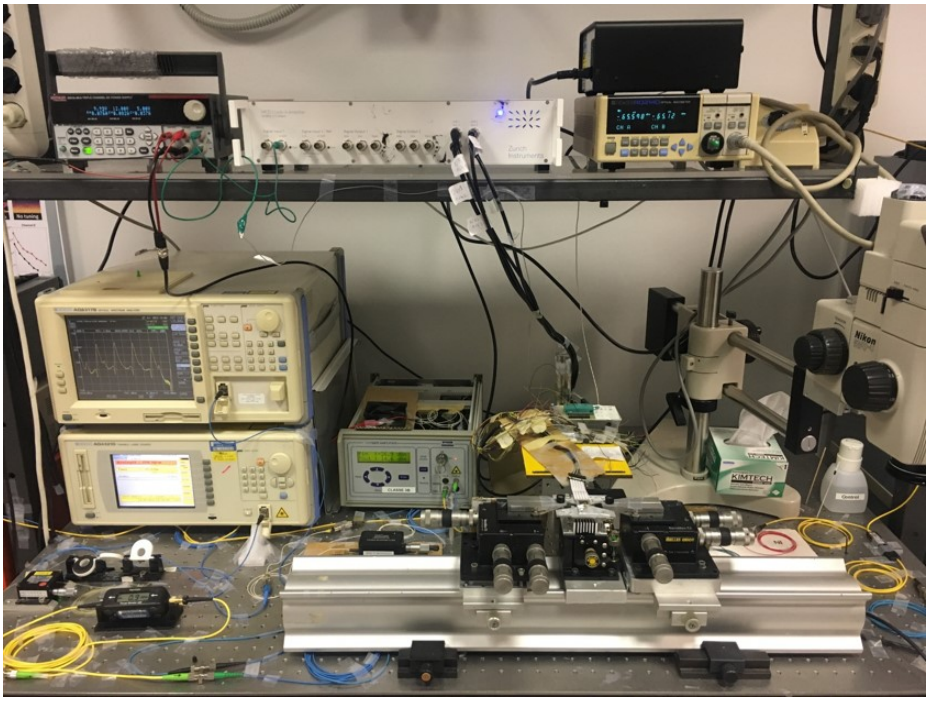


Figure 3.4: Picture of test bench

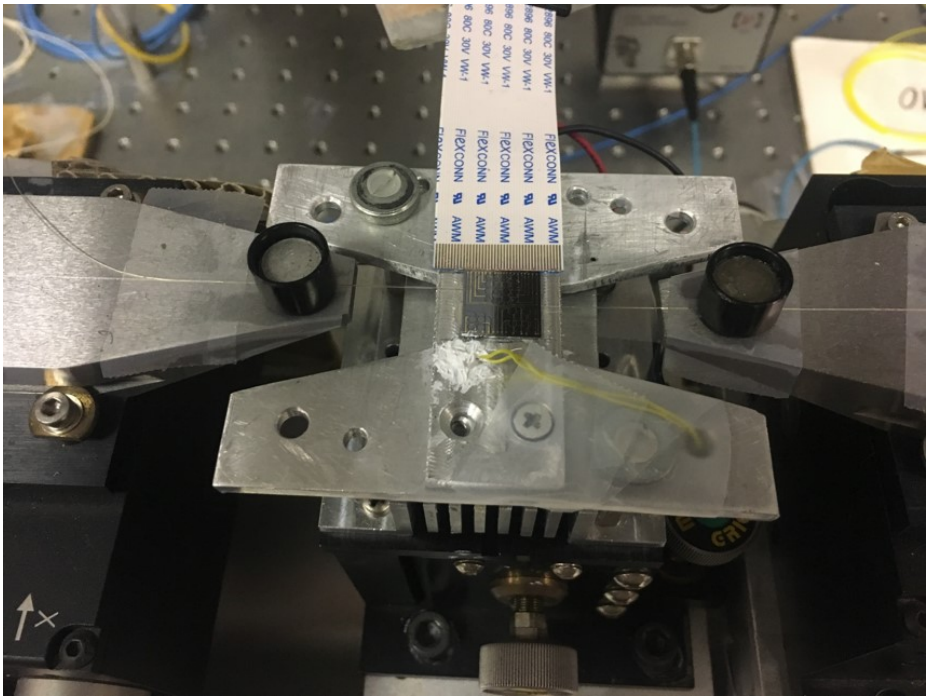


Figure 3.5: Picture of chip bonded and mounted on a TEC

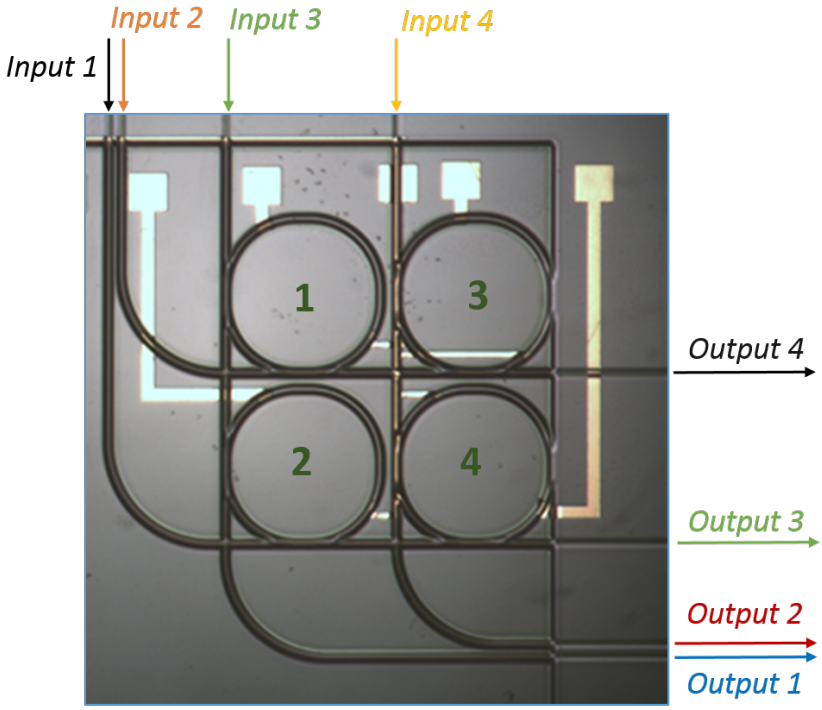


Figure 3.6: Microscopic view of mesh of 4 MRRs in SiON technology

### 3.3.1 Comparison between individual and TED-based tuning

First set of experiments belong to validating effectiveness of TED tuning algorithm on the chip under test in presence of thermal cross talk. Conventional tuning methods for these kind of filters exploit sequential sweeping of individual resonance of each MRR to locate them into desired wavelength (here referred as individual tuning). Without loss of generality, we assume cross talk induce equal phase coupling $\mu$ between neighboring MMRs on the chip, so the phase coupling matrix is as indicated in the previous chapter, as follow:

$$T = \begin{pmatrix} 1 & \mu & \mu & \mu \\ \mu & 1 & \mu & \mu \\ \mu & \mu & 1 & \mu \\ \mu & \mu & \mu & 1 \end{pmatrix}. \tag{3.1}$$

Without further duplication of concepts, the eigenvectors of current structure is

as calculated earlier:

$$P = \begin{pmatrix} \frac{-1}{4} & \frac{3}{4} & \frac{-1}{4} & \frac{-1}{4} \\ \frac{-1}{4} & \frac{-1}{4} & \frac{3}{4} & \frac{-1}{4} \\ \frac{-1}{4} & \frac{-1}{4} & \frac{-1}{4} & \frac{3}{4} \\ \frac{1}{4} & \frac{1}{4} & \frac{1}{4} & \frac{1}{4} \end{pmatrix}. \tag{3.2}$$

The test is executed with 10 random initial phases intentionally introduced to heaters. At input port 4 an optical signal modulated with 10GHz On-Off Keying (OOK) is injected to the chip.
To point out the benefit of TED method, the experiment was initiated for both TED-based and individual-based tuning algorithm to compare the results. Needless to say, the initial random points are identical in both cases. The filter is tuned by using the procedures described in the previous chapter and the goal is defined based on maximizing the output power at port 3. The process is stopped after 40 iterations in each trials. Figure 3.7 illustrates the convergence curves in both cases. Blue-solid lines are TED-based and red-dashed lines are individually-tuned cases. As shown in the figure, TED-based trials have converged to goal output power after maximal 20 iterations. But in individual tuning approach, not only they plead for more iterations to converge but also suffer from instability issues and in some cases they are not even converged to goal point and keep oscillating.

### 3.3.2 Single and double channel routing

Photonic networks-on-chip (NoC) has recently gained popularity as a practical substitute for traditional electrical interconnects for next generation of chip multiprocessors (CMPs)[37]. Global metallic interconnect delays increase exponentially and becoming a bottleneck for improving the performance of CMPs, Hence the optical interconnects have broader bandwidth and lower latency compared with that of electrical ones [32, 54].
By utilizing an optical network to link multiple processors the full capability of large on-chip parallel systems can be obtained [8]. However, a major task in any network is the ability to route and switch. Routers perform the duty of dynamically select the destination for the input source.
Network of interconnected MRRs are considered as a hitless scheme to design passive routers, in which perform by routing signals based on their wavelength [84, 99]. They may well be exploit in WDM systems as an optical add/drop multiplexer (OADM).

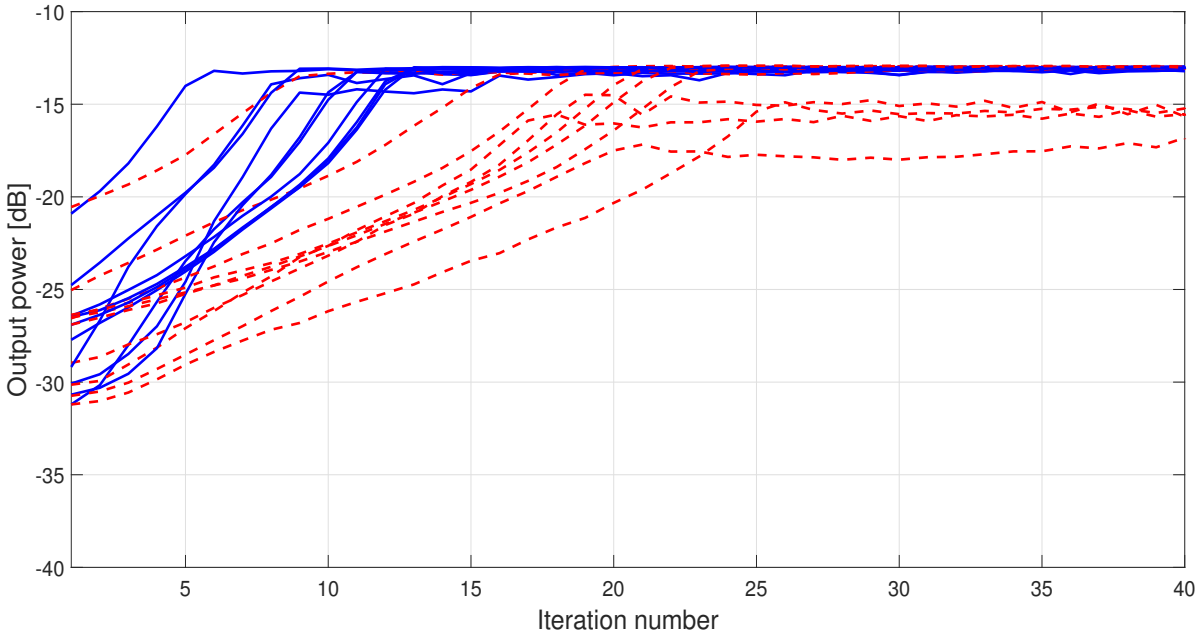


Figure 3.7: Output power variation in TED versus individual tuning methods. (red dashed lines are individually-tuned & blue solid lines are corresponding TED)

Interconnected MRRs in proposed structure are particularly useful since they can be tuned to filter a specific wavelength and pass it along to different waveguides and doing so, switch the direction of input light.
When the resonance condition of MRR is met (as quantified in second chapter), input signal is switched and consequently light is passed to the drop port instead of the through port.

In this part, we practically assess the ability of purposed structure of interconnected MRRs to route the source signal.
The first experimental test is dedicated to single channel routing. Ports 4 and 3 are chosen as input and output ports, respectively.
The modulated signal spectrum entering the chip exploits MRRs number 3 and 4. As a result, the filter's transfer function is foreseen to have a notch corresponding to resonant wavelength of 3rd MRR and a peak match with that of 4th MRR.

Experiment is initiated for 10 different perturbed cases. These cases are defined by introducing 10 random sets of voltages to heaters mounted on top of MRRs, through pads. These values push heaters to different points, thus forming diverse transfer

functions as shown in Figure 3.8.

Input signal is lunched with specific central wavelength and the algorithm is executed inside MATLAB whilst controlling the chip via Zurich instrument. The numerical simulator objection is defined based on maximizing the output of port 3, in such a way that in each iteration, output power is sampled and compared with previous step and the numerical function is designed to increase it.
Hence a singular maximum point exists, we expect the filter's transfer functions in all 10 trials, converging to almost same point.
However, it should be noted that applied voltages are restricted to certain values, to prevent burning out heaters. This obligation puts limitation on the filter's tunability range.
Figure 3.9 shows the fine-tuned frequency response of filter for all considered cases after implementation of TED algorithm. As expected, regardless of initial status of transfer functions, all 10 cases have converged to almost same spectra.

Next scenario is defined for two different channels in input spectrum, and the objective is routing them to two different output ports. The peculiar asset here is the capability of doing so by only detecting and sampling of one output.
For this purpose, we employ frequency labeling technique[7]. To investigate this technique, more involved setup is required. The scheme of new arrangement is depicted in Figure 3.10

As disclosed in the scheme, two optical sources are required in order to produce two different optical channels. The technique outline, works based on applying labels to these different optical wavelengths and route them to different outputs. These labels are local low frequency signals (different from each other) shallow modulating the optical carriers.
To further clarify, we refer to Figure 3.10. Laser number one is OOK-modulated with 10GHz data-signal and later it is labeled with a low frequency signal (100KHz) denoted as *label1*. In the second branch, CW channel is only modulated with low frequency tone signal (300KHz) denoted as *label2*. Afterwards, these 2 optical signals are combined together and pass through the rest of the arrangement which is identical to prior setup.

Upon exiting the chip, optical signal is fed to a photodetector, and turns into an electrical signal consists of two different frequencies each exposing different labels.

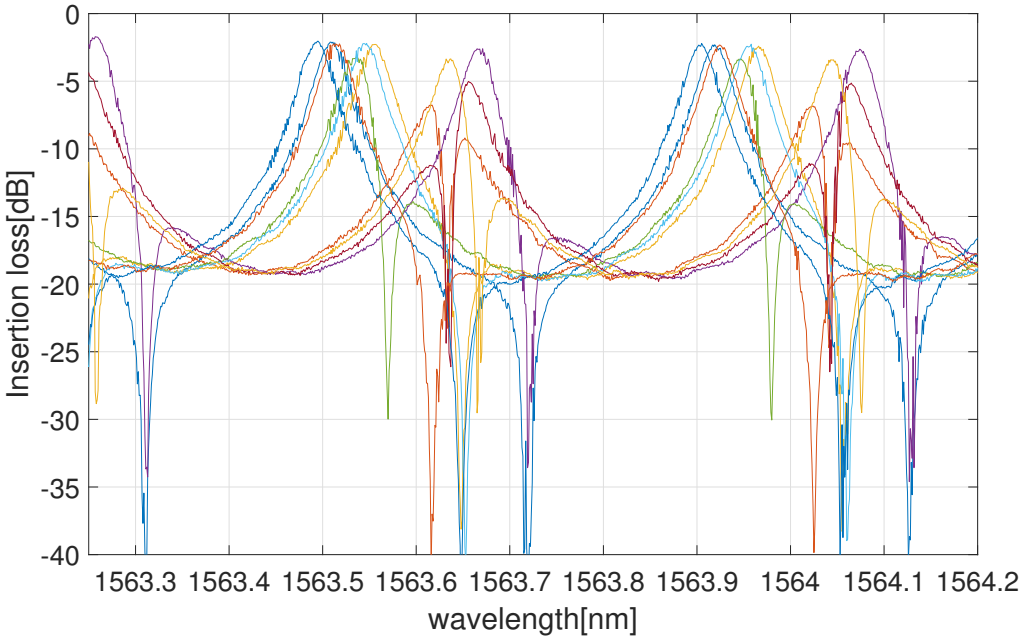


Figure 3.8: Initial random transfer functions

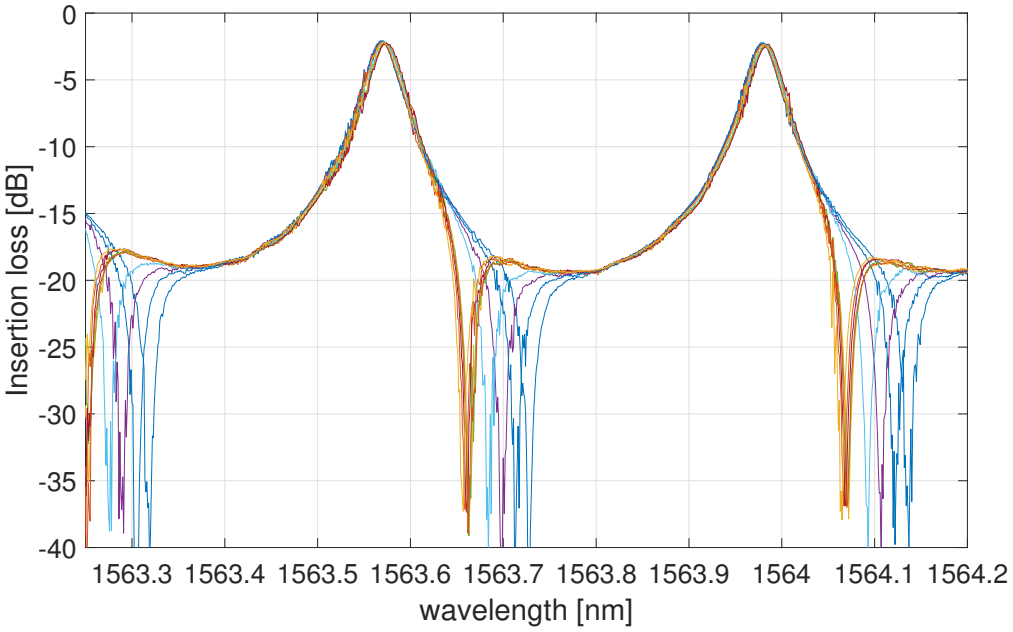


Figure 3.9: fine-tuned transfer functions

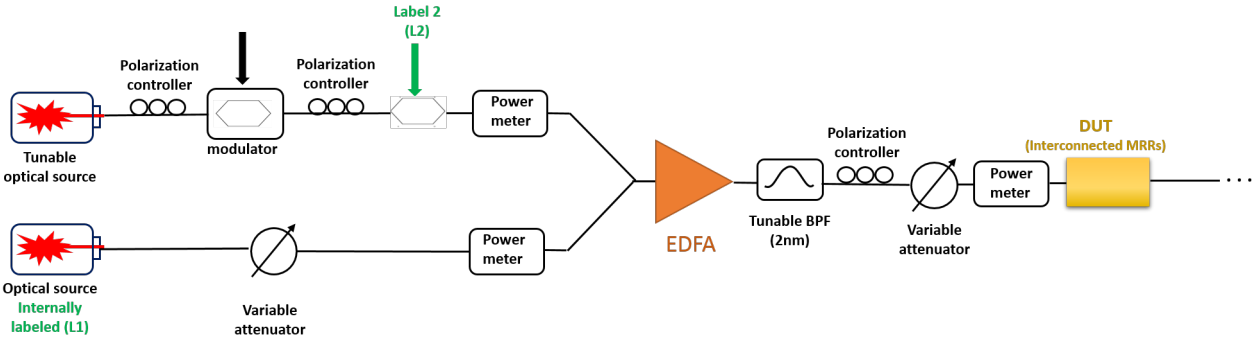


Figure 3.10: Schematic of setup for routing two channel spectra

Finally this electrical signal is demodulated with label signals frequency via Zurich instrument, and therefore amplitudes of them are separately distinguishable in order to tune each MRR to a different optical channel.

The optical path inside chip is depicted in Figure 3.11. With reference to Figure 3.11, input channel enters the router (mesh of MRRs) through input port 2. The objective here is to route $\lambda_1$ which corresponds to optical channel identified with label1 to output 4 and route the optical channel with label2 ($\lambda_2$) to output 3.
To achieve this goal, resonance wavelength of MRR3 should correspond to optical channel 1 and resonance wavelength of MRR4 should match with that of channel 2. Meeting this condition, $\lambda_1$ and $\lambda_2$ are routed to MRR3 and MRR4s drop ports, respectively.
Since the only monitored signal is output 3, the goal function is defined based on maximizing the following condition:

$$\lambda_2 - \lambda_1. \tag{3.3}$$

Since input optical signal passes through a filter with one notch and one peak in its transfer function, the only means to reach the target point, is to set local maxima on $\lambda_2$ (MRR4 dropping $\lambda_2$) and local minima on $\lambda_1$ (MRR3 dumps $\lambda_1$ in its through port) .

10 set of randomly chosen voltages have been applied to heaters as the initial points, defining the goal function to maximize the difference between amplitude of label2 and 1.

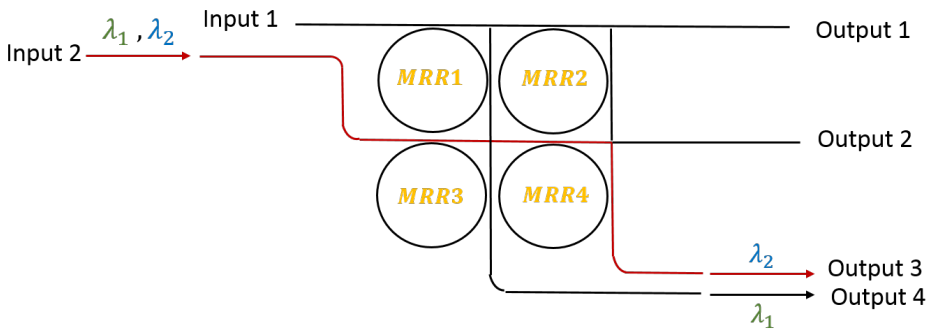


Figure 3.11: Schematic of chip in case of routing 2 different optical channels.

It is important to note that the present experiment relies on using labeling technique, as a method to read the amplitude of channels separately and define a goal function to achieve a unique transfer function as the result.

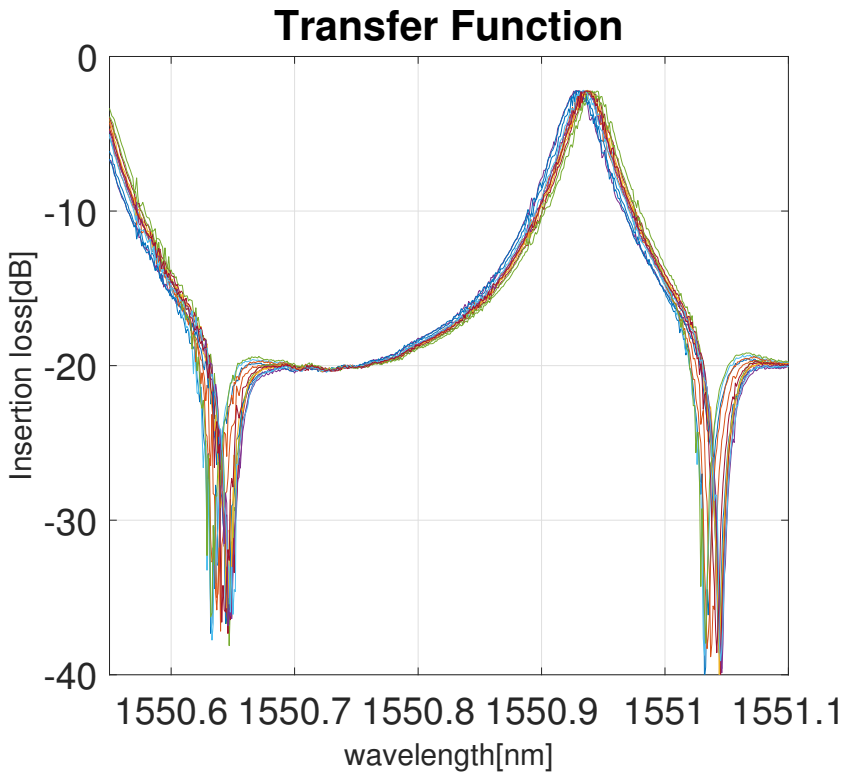


Figure 3.12: fine-tuned transfer function of filters in case of two-channel routing

needless to say, several channels could be selected and directed through different outputs, exploiting adequate error function.

### 3.3.3 Disconnected thermoelectric cooler (TEC) experiment

Up to this point thermoelectric cooler (abbreviated as TEC) with a close loop controller, has been a inseparable part of our setup bench. TEC-controller maintains overall temperature of chip constant through the Peltier effect. Therefore the chip is immune from undesirable impact of heat gradient due to heaters and ambient temperature variation.
In this section we resolve to evaluate the set up performance while disconnecting the TEC controller. As the feedback control is constantly on, it is presumed that the algorithm itself should compensate for absence of TEC-controller leading to harsh temperature variation of chip. As the temperature of chip keep rising up, it is expected from control scheme to decreases the overall applied electrical power to the heaters in order to maintain the filter's transfer function in its desired position and neutralize the temperature boost overall the chip.

The experiment is performed for 7 random trials. As before, a random function choses initial points for heaters and then algorithm is executed to guide heaters to their correct values. Initial temperature in all the cases is 25 degree as previous tests. Figure 3.13 discloses the final result with final temperature of the chip in each trial. Within almost 40 iterations, All the the transfer functions has reached optimum point. The experiment is continued to monitor the variation of chip temperature and the performance of algorithm alongside, to test its robustness.

Figure 3.13, suggests that as temperature raises up, voltage values injected to heaters evolve themselves to maintain the power nearly constant, slightly oscillating close to optimum point's power. Final results, attests the strength of algorithm for compensation in case of TEC absence.

It is important to mention, since on-line operation of TEC leads to high power consumption, capability of disconnecting it from the system saves notable amount of power.

It is another significant advantage of TED over other techniques, as its fast and transparent tuning mode, allows designer to further reduce power consumption inside PICs package.

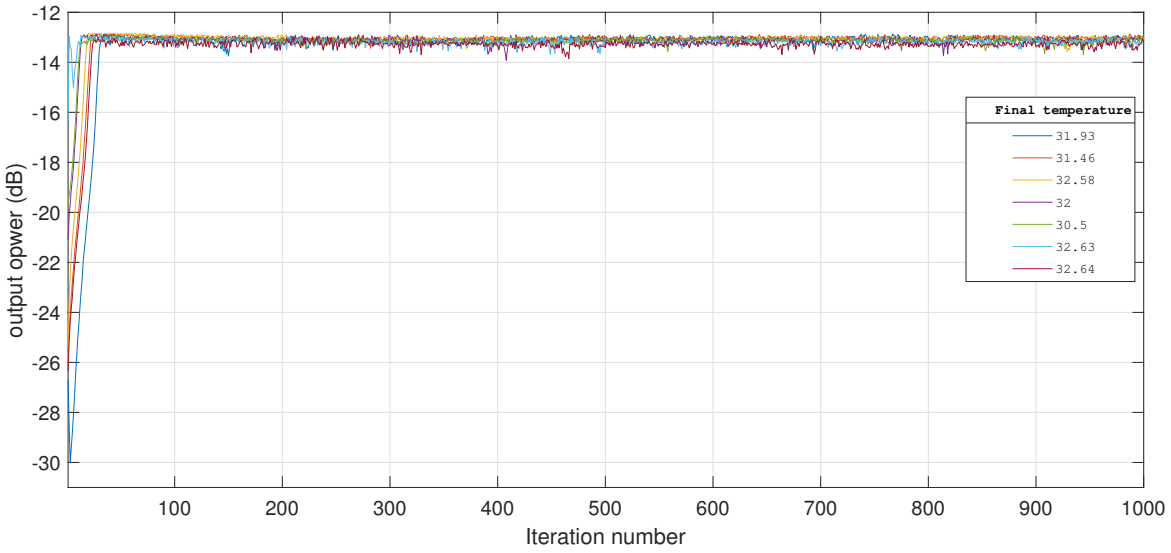


Figure 3.13: Output power variation in case of disconnected TEC-controller for 7 different trials

# Chapter 4

# Adaptive and tunable bandwidth filters

The aim of this chapter is to apply TED technique on a more sophisticated structure, consists of a Mach-Zehnder interferometer (MZI) loaded by two MRRs in all-pass configuration. This structure is identified as a tunable bandwidth filter.

First part starts with introduction on reconfigurable filters and their property (tunability and adaptation), followed by expressing their significant roles telecommunication systems.

The second section is dedicated to surveying effectiveness of TED method on the proposed structure. The objection is defined based on reconfigurability of the filter. Through simulation and experimental tests, TED technique succeeds in tuning and adapting filter's bandwidth to the input signal spectrum.

## 4.1 Reconfigurable filters

Optical filters are one of the key components inside photonic integrated systems, like wavelength division multiplexing (WDM) networks, as they are recently taking over as the chief technology in point-to-point transmission links[80],microwave photonics[59][53]and optical communication systems[16].
Optical filters are used to separate the desired channel from rest of the band. Adaptation to input signal wavelength and bandwidth are two desired key features, allowing minimizing the pulse distortion and maximizing the signal to noise ratio (SNR), as well as adjustment to different bit rates[14].
Many different techniques have been proposed for filter design[52][46][70][67].However, for obtaining flexibility in bandwidth and central wavelength, more involved techniques are required. For instance, one proposed method is tuning coupling sections of MMR[93][10] to achieve bandwidth tunability. The drawback presented in such structure is the limitation in bandwidth tunability. Another approach is based on a single MMR tuned by micro-electronic-mechanical-system (MEMS)[40][93]. This method also appears to be power thirsty as to realize MEMS tunability, an actuation voltage of 40v is required. In other demonstration, an optical bandwidth tunable filter is proposed based on liquid crystal technology[98], Which by controlling the voltage of liquid crystal chip array, the phase of incident light is modulated and changes the polarization state of incident light and in the output after passing through the polarizer, each wavelength is treated differently leading to bandwidth variation. Another relatively common approach is to embed MRRs in an unbalanced Mach-Zehnder Interferometer (MZI) which enables large bandwidth tunability[14][77][3]. For exploiting bandwidth tunability, thermal actuators are triggered to modify the phase and coupling coefficient of MRRs. In this chapter we study the same structure as stated before [58].

In the current structure, three active actuators are executed. With aid of these actuators and implementing TED, we fine-tune the bandwidth and central wavelength of the filter.

The filter structure is shown in Figure 4.1. The unbalanced MZI consists of 3dB couplers in input and output. Two MRRs are in all-pass configuration with circumference equal to $L_r$ . The length of unloaded arm of MZI is set to have optical length difference equal to $L_r$ to match the Free Spectral Range (FSR) of MRRs and MZI. Power coupling coefficient between MRRs and MZI arm is equal to $K_r$.

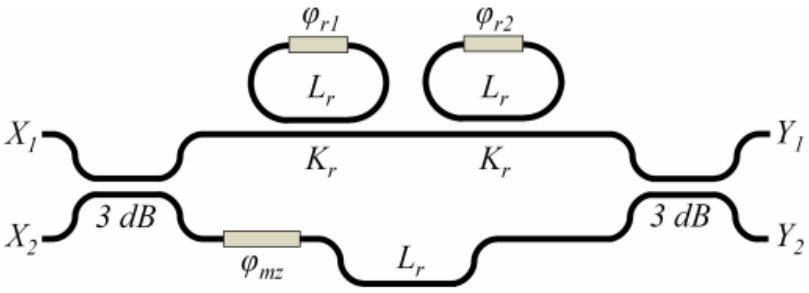


Figure 4.1: Schematic of tunable bandwidth filter.

As mentioned earlier, bandwidth and wavelength tunability is realized by active control of heaters mounted on MRRs and MZI arms, respectively. Heaters (phase shifters) are shown by gray boxes in Figure 4.1. Altering voltage of heaters in MRRs induced phase difference of $\Delta\phi = \phi_{r2} - \phi_{r1}$ , which control the 3dB bandwidth, while the condition $\phi_{mz} = m\pi + (\phi_{r2} + \phi_{r1})/2$, (m is an integer) maintains the filter transfer function always symmetric with respect to filter central wavelength. Adding any phase to phase shifters changes the filter characteristic function, and varying $\phi_{mz}$, swap the through and drop ports transfer functions.

Figure 4.2 depicts simulation results changing $K_r$ from 0.65 to 1 and $\Delta\phi$ from $0 to 2\pi$ and measuring the corresponding values of 3 dB bandwidth, off-band rejection and shape factor. The off-band rejection and the shape factor are shown as a function of $K_r$ and of the 3 dB bandwidth normalized to the filter FSR. Level curves are also drawn to help reading the different values of the color-map. The two maps show that the range of bandwidth tunability caused by variation of $\Delta\phi$ from $0 to 2\pi$ reduces as the coupling coefficient increases. The limit case is represented by $K_r = 1$ where the two MRRs act as pure delay lines and the filter transfer function is that of an unbalanced MZI independently of $\Delta\phi$ Focusing attention on the off-band rejection, Figure 4.2(a) illustrates that an overall increase of this figure of merit can be obtained increasing $K_r$ . A trade-off is therefore needed to obtain both wide bandwidth tunability and a fair off-band rejection for all of the filter configurations. In the trade-off, filter shape also has to be taken into consideration. Increasing the MRR coupling coefficients flatten the shape of the filter thus reducing the shape factor Figure 4.2(b). An upper limit for $K_r$ can be given by this parameter depending on the required performance. These maps allow the designer to choose the value of $K_r$ corresponding to desired

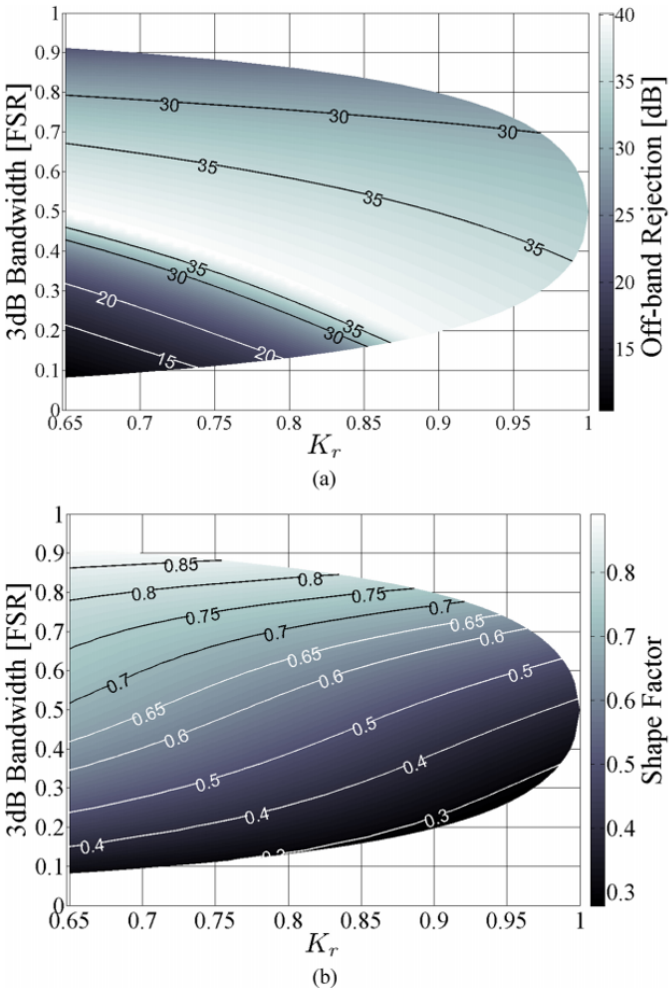


Figure 4.2: Map of the (a) filter off-band rejection and (b) shape factor (color bar and contour lines) for the 3 dB bandwidths obtained for $0 < \Delta\phi < 2\pi$ (y axes) as a function of $K_r$ (x axes).

performance providing at the same time a general view of the mutual effect of the parameters.

## 4.2 Numerical simulation

In this section we perform numerical simulation regarding the structure introduced, to verify the filter tunability for different input signal spectrum. Similar to previous study, the software used for modeling is a MATLAB script.

### 4.2.1 Tuning Mach-Zehnder loaded by two MRRs

In this part, we investigate the ability of TED algorithm to fine-tune the introduced structure, and checks it's performance in adapting filter's bandwidth to the channel spectrum.

Before initiating the numerical simulator, we need to extract the phase coupling matrix and further the eigenvectors of the structure to exploit TED technique. To further simplify the algorithm, we assume same coupling coefficient between heaters mounted on top of chip referred as $\mu$.

Matrix below describes the phase coupling between heaters with reference to Figure 4.1:

$$T = \begin{pmatrix} 1 & \mu & \mu \\ \mu & 1 & \mu \\ \mu & \mu & 1 \end{pmatrix} \tag{4.1}$$

followed by:

$$P = \begin{pmatrix} -1 & -1 & 1 \\ 1 & 0 & 1 \\ 0 & 1 & 1 \end{pmatrix} \tag{4.2}$$

adapting eigenvector matrix of the structure, in tuning process promise an uncoupled compensations. So taking steps in these direction would not perturb neighboring heaters.

to survey this ability, some random initial phases are introduced to the heaters and the TED algorithm is executed to compensate for the perturbations. Figure 4.3 shows 10 random initial transfer functions for the filter. The input signal is OOK-modulated and hold 6GHz of bandwidth. regardless of initial perturbed filter shapes, we expect all the heaters to converge to almost the same voltages, thus displaying identical final transfer functions. Figure 4.4 depicts the final shape of 10 random filters, and as predicted all of them have been converged to the same transfer functions. The final spectrum of filter maintains about 14GHz of bandwidth.

Another set of simulation is performed to investigate the capability of filter to adapt to input signal spectrum. As mentioned in the introduction part, flexibility is a key property required in the future telecomm and datacomm networks. The data

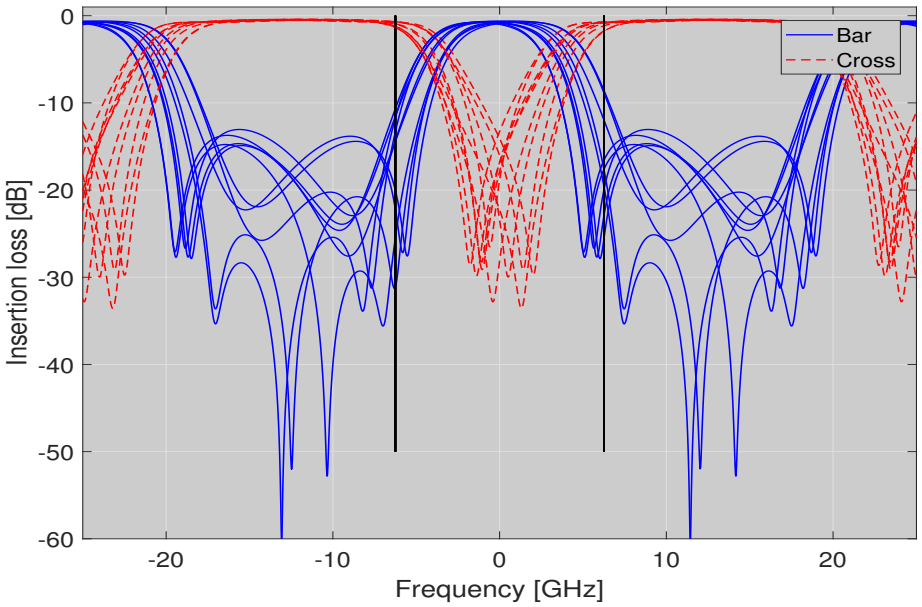


Figure 4.3: 10 initial points for filter transfer functions

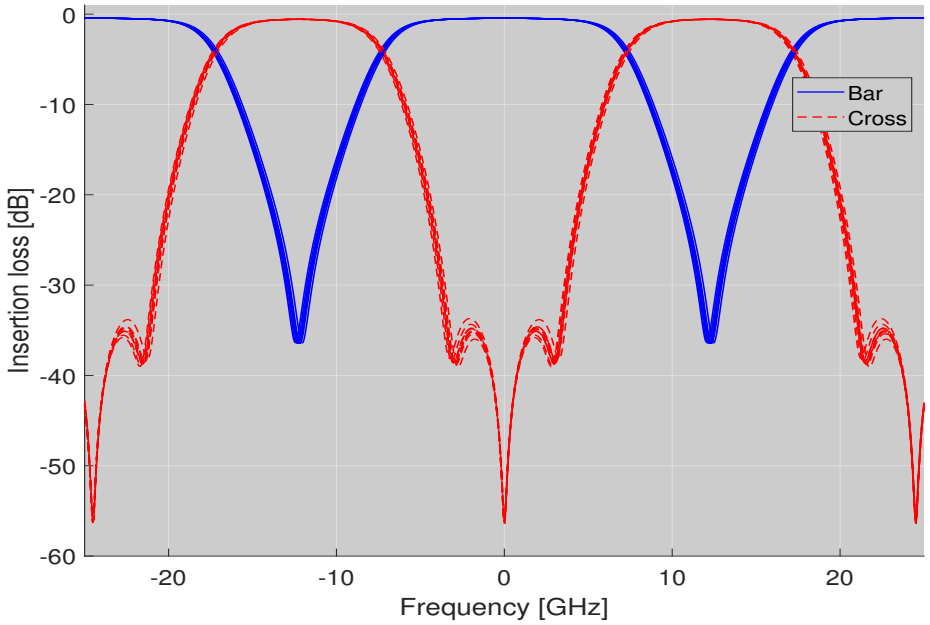


Figure 4.4: Fine-Tuned transfer functions for input spectrum with 6GHz bandwidth

flow of a system is not necessarily constant, and a desired property of optical filters is ability of adaptation to input signal bit rate and bandwidth, so to maintain the

SNR of filter as high as possible.
For the first trial, an OOK-modulated signal with bandwidth of 10GHz is chosen. The procedures is as before, so 10 random initial points are introduced to heaters and then the TED is utilized to compensate for the errors. Figure 4.5 demonstrates fine-tuned transfer functions.

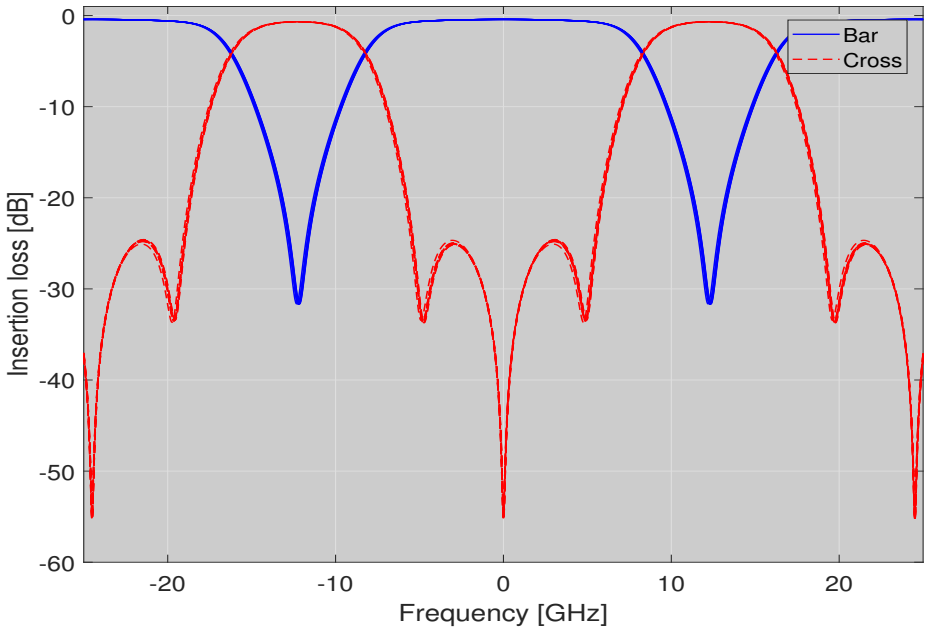


Figure 4.5: Fine-Tuned transfer functions for input spectrum with 10GHz bandwidth

As expected, by increasing the input signal bandwidth, the filter adapts itself to a higher bandwidth. In the recent case, filter has adapted itself to bandwidth of 16GHz.

The last set of simulation result is performed for a new modulation scheme to validate TED performance in different configuration. Input optical carrier is QPSK-modulated with a 22GHz of spectrum. Figure 4.6 demonstrate the initial perturbed and fine-tuned filters. The final filters are all converged to about 17GHz.
It is necessary to mention that the gap between obtained result and input spectrum bandwidth is due to filter tuning range limitation which is maximally 17GHz, therefore TED proves its substantial functionality by pushing heaters to modify filter towards its maximum bandwidth.

So far, the effectiveness of TED-algorithm on the presented structure by means of simulation has been proved. The next step requires to validate the obtained results in a experimental test to fully prove the ability of TED in adapting the filter spectrum.

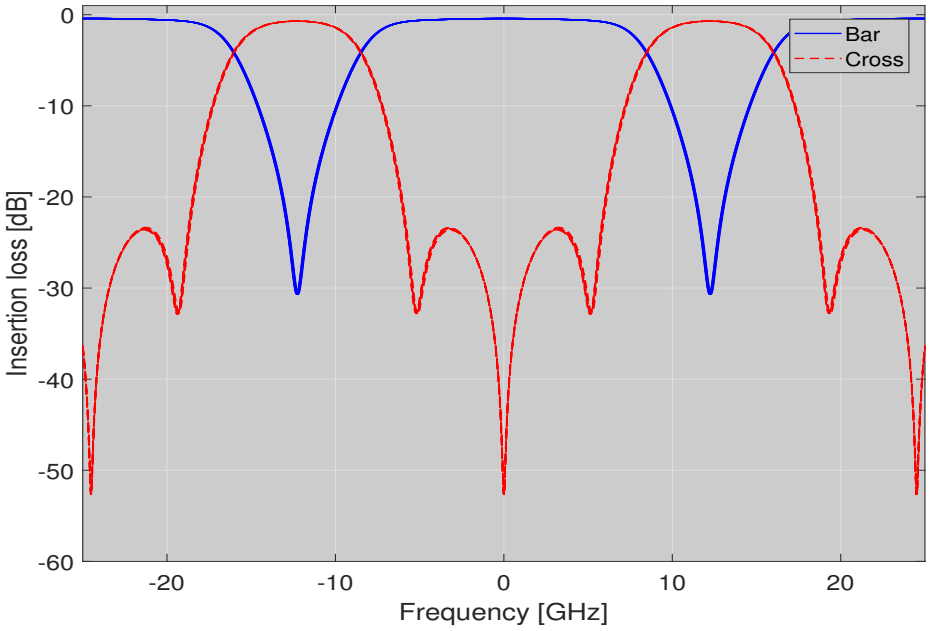


Figure 4.6: Fine-Tuned transfer functions for QPSK-modulated signal with 22GHz bandwidth

## 4.3 Experimental results

In this section, experimental analysis are performed to practically validate the simulation results and confirm the functionality of TED in this very structure to be exploit as a tunable bandwidth filter.

The experimental setup is the same as illustrated in 3rd chapter. The waveguides are in SiON technology. On top of each element, a Chromium heater is mounted and they are connected to the pads through tracks made of Gold.

A top view of the filter is shown in Figure 4.7. White lines are the gold metal tracks connecting the heaters to the pad. The approximate length of Mach-Zehnder arm is 6mm as indicated in the figure. No further modification has been introduced to test bench and it is identical to previous illustration.

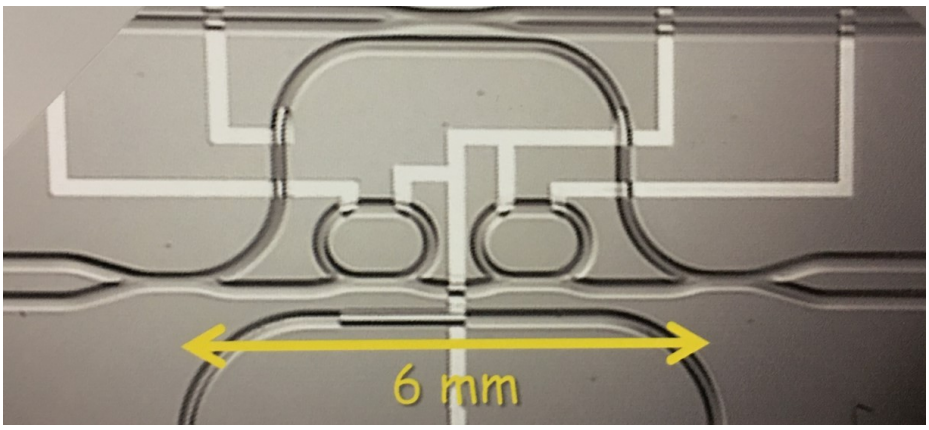


Figure 4.7: Top view of the chip

### 4.3.1 Compensating initial perturbations

Identical to previous experimental tests, 10 set of random perturbations are injected to circuit as input voltage for the heaters. These initial values fluctuating between -5 to 10 volts in which corresponds 0 to 15 volts.
The close loop reference point used to tune the bandwidth, as explained in the simulation part, is based on obtaining minimum output power in the cross port of the filter.
The input optical carrier is OOK-modulated signal with 6GHz bandwidth. Initial shapes of 10 filters' transfer function is depicted in the Figures 4.8 and 4.9.

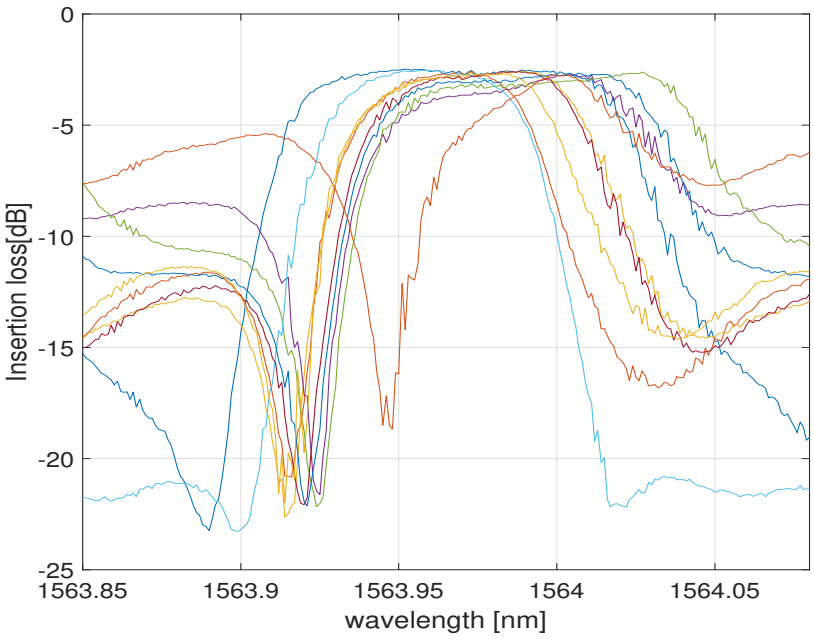


Figure 4.8: Initial perturbations in bar port

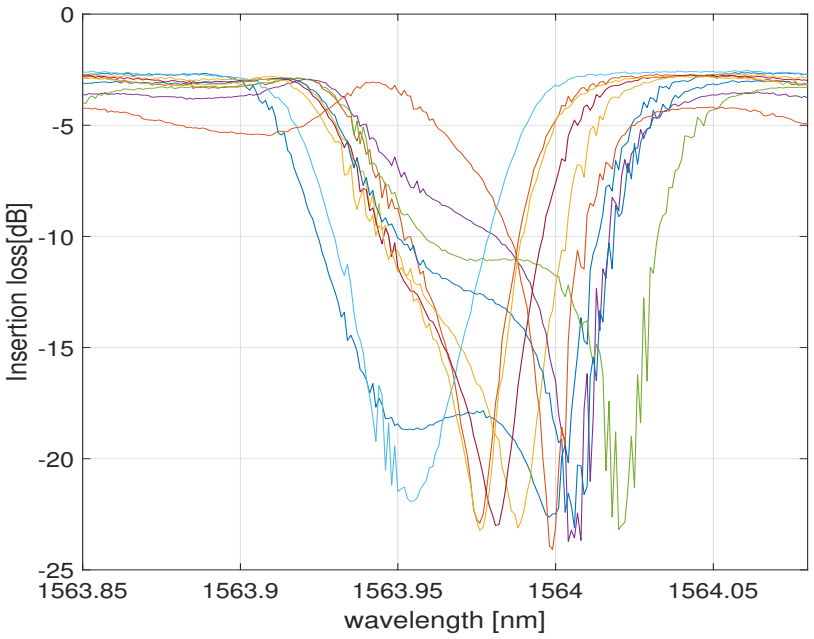


Figure 4.9: Initial perturbations in cross port

After performing the tuning algorithm using TED method, all 10 trials have converged to the same curves for the transfer function. The fine-tuned transfer function

of filter in both bar and cross ports is demonstrated in Figures 4.10 and 4.11, respectively.

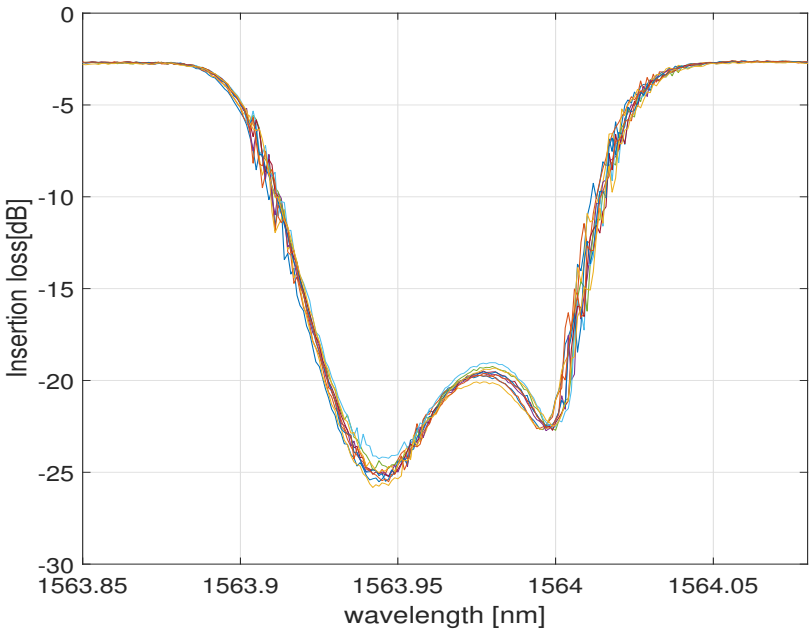


Figure 4.10: Fine-tuned transfer function of cross port in case of 6GHz input spectrum

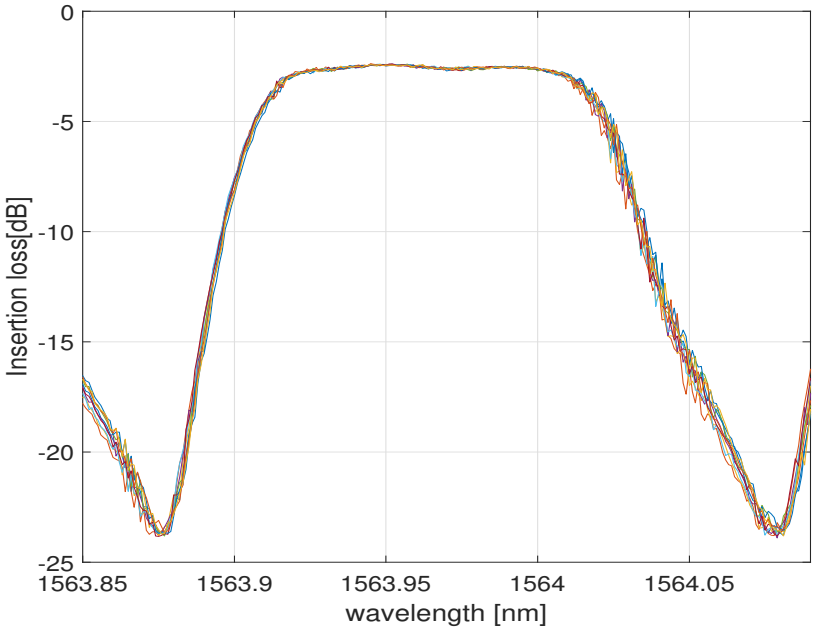


Figure 4.11: Fine-tuned transfer function of bar port in case of 6GHz input spectrum

The final filter (bar port) is converged to 14.4GHz, so the objective is met and the 6GHz modulated signal can perfectly passes through the filter.

### 4.3.2 Adaptation to the channel spectrum

For the future dynamic networks, one critical property of filters is the potential of adapting to bandwidth of input spectrum. One significant property of proposed filter is the ability to adopt its bandwidth to input channel spectrum. By means of TED method, filter is capable of spontaneously modify its bandwidth to that of input spectrum.

In our experiments, the sampled signal which enters the feedback loop is the output of the cross port multiplied by the input signal. The mathematical model based on TED is then applied to the chip via Zurich instrument to minimize the feedback signal. Evidently, the minimal condition happens when the bandwidth of bar port matches (or exceeds) bandwidth of input signal.

We examine the dynamic behavior of filter for two different input signal spectrum comprised of 10GHz OOK-modulated scheme and 22GHz QPSK-modulated signal. As predicted, in each condition, the transfer function of filter modifies itself to match with the input signal bandwidth.
The procedure of performing the test is as before. Figure 4.12 and Figure 4.13 illustrate final transfer functions of bar and cross ports of filter in case of signal with 10GHz spectrum. the final filter is converged to about 14GHz.

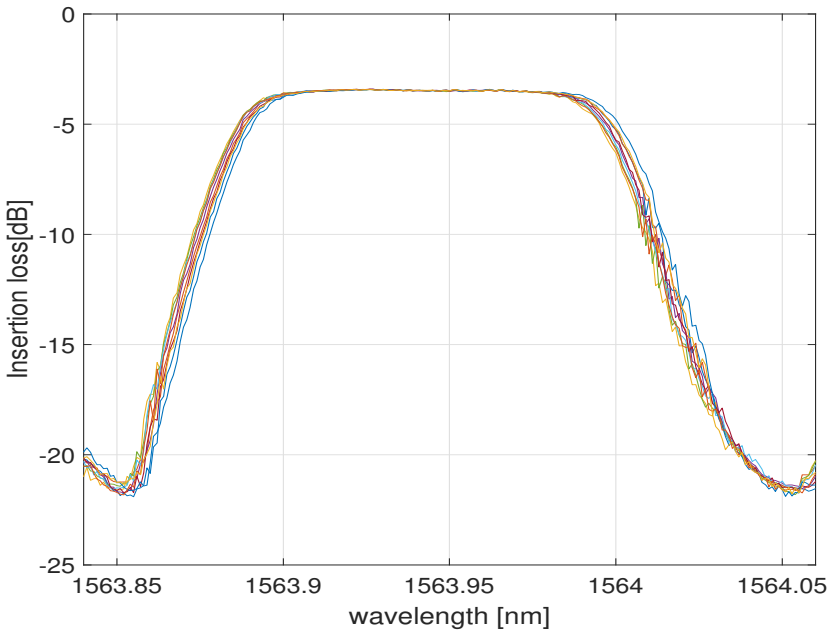


Figure 4.12: Fine-tuned transfer function of bar port in case of 10GHz input spectrum

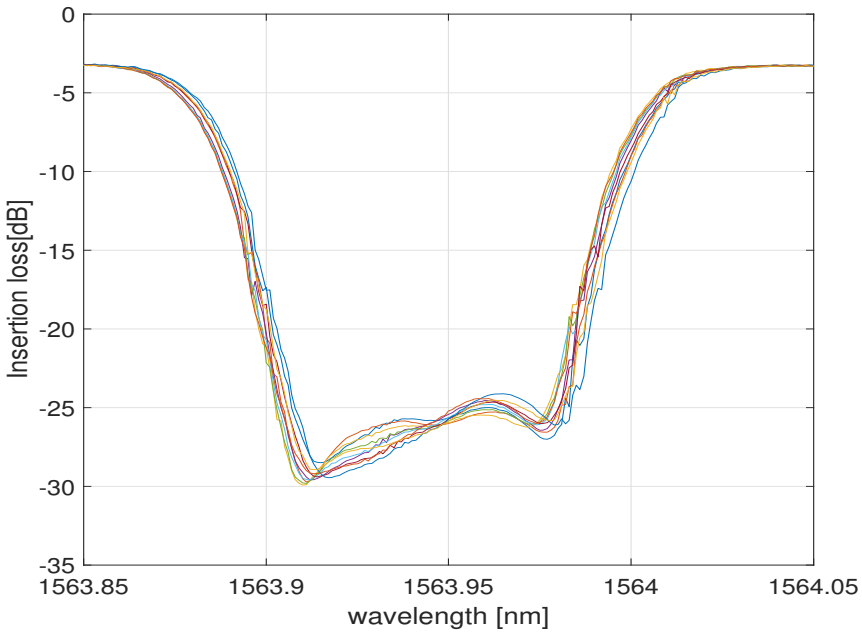


Figure 4.13: Fine-tuned transfer function of cross port in case of 10GHz input spectrum

For the second case with input spectrum of 22GHz, further clarification is entailed. As indicated before, the filter has the capability of enlarging its bandwidth to maximum value of 17GHz, hence as we survey the case we expect to obtain the largest feasible bandwidth of the filter. Figure 4.14 and Figure 4.15 respectively demonstrate bar and cross ports of fine-tuned filter. Obtained bandwidth is about 17 GHz as predicted.

The results show that the automatic resonance alignment system behaves in agreement with the simulations.

Abrupt variation in input spectrum is a quite extreme case of perturbation. Online adaption of TED mechanism on the photonic integrated chip, prevent adverse degradation of the system in case of sudden modulation or bandwidth change since TED compensates for such issues by following input spectrum change.

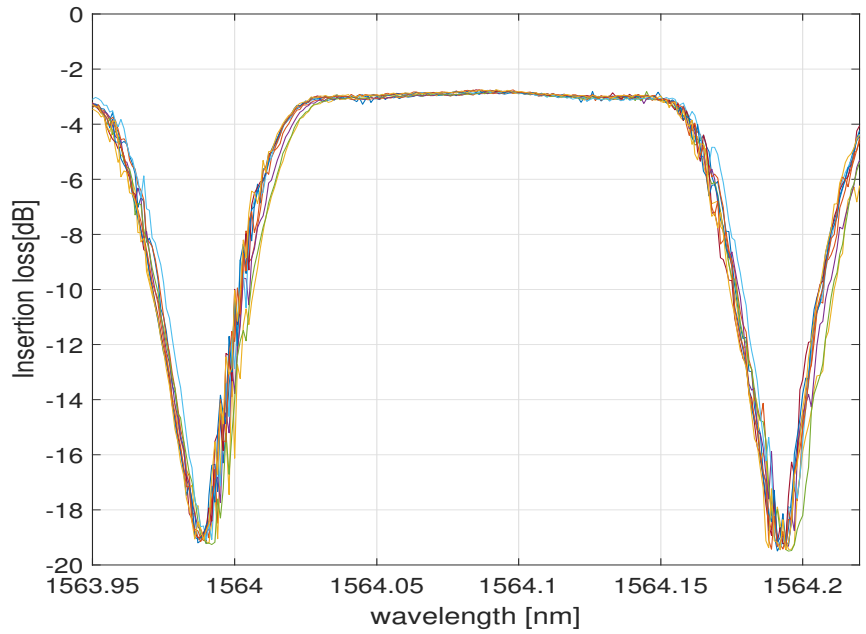


Figure 4.14: Fine-tuned transfer function of Bar port with 22GHz input signal spectrum

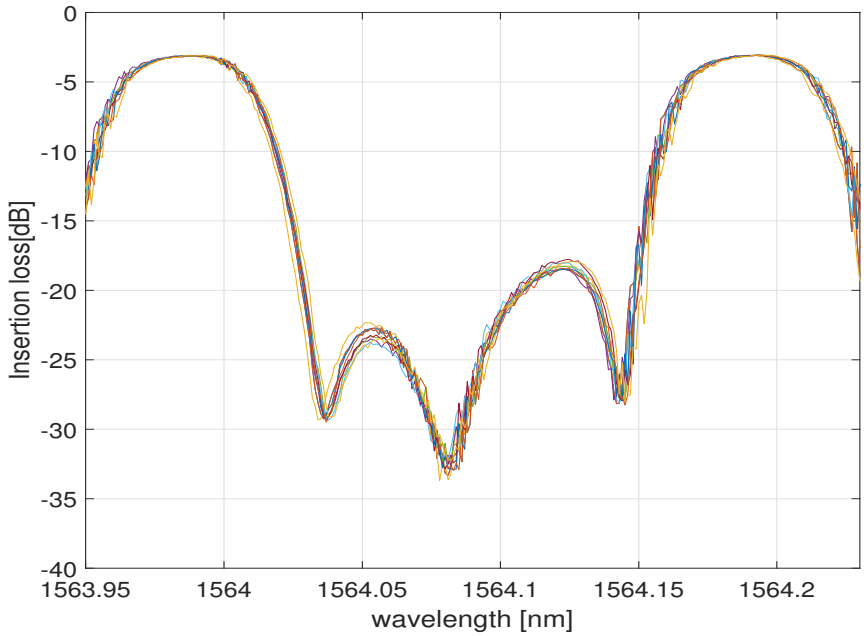


Figure 4.15: Fine-tuned transfer function of cross port with 22GHz input signal spectrum

# Conclusion and Discussion

In this thesis, we theoretically introduced and experimentally demonstrated a technique capable of canceling the phase coupling induced by thermal cross-talk in photonic integrated circuits. Instead of individual control of actuators, in TED technique all the actuators are controlled simultaneously according to appropriate weights, which are based on eigen solution of the thermally coupled system. Mathematically, this implies a deterministic coordinate transformation which can be adapted to any kind of tuning and locking algorithm, for instance on look-up tables, gradient-based and dithering-based techniques, as well as multi degree of freedom (DOF) stabilization methods. The use of the TED technique is not limited to specific circuit topologies but can be extended to generic PIC architectures. Through numerical simulations we proved its effectiveness in two different structures. A Mach-Zehnder interferometer loaded with two microring resonators which functions as a tunable bandwidth filter, and a mesh of 4 microring resonators exploited as wavelength switching scheme. While in individual control of phase actuators the thermal cross-talk can inhibits convergence, adopting the TED method, convergence is always achieved in our simulations and experiments. Furthermore, the TED-based tuning technique allows to reduce average number of required iterations while this number is also less sensitive to the initial perturbed state of the PIC. Experimental results performed on MRR-based filters confirm the faster and more robust convergence of the TED-based tuning algorithms, with respect to conventional approaches, to counteract temperature drifts or to track random fluctuations of the wavelength of the input signal. The material platform in which we test the TED tuning based algorithm was high-index-contrast silicon oxynitride (SiON) platform. Moreover TED has the capability of adaptation to different photonic integrated chips and platforms.

In this thesis following functionalities are validated using TED-based tuning method, briefly pointed out as:

- Fine-tuning the transfer function of the structures in both chips, and comparing individual and TED-based tuning and verifying superiority of TED-based method over conventional individual-based tuning schemes in term of speed and accuracy.

- Routing input signal spectrum into two different output ports using labeling method in mesh of 4 MRRs by adapting TED-technique.

- Performing tunning and locking experiment while disconnecting thermoelectric cooler device from the system which maintains the overall temperature of the structure constant.

- Demonstrating capability of adapting reconfigurable filter bandwidth and central wavelength in MZI loaded by MRRs, to input signal spectrum using TED technique.

# Future work

It should be noted that, although TED method here is introduced to cope with the certain problem of thermal cross-talk, its validity can be extended to the other cross-talk effects, such as mechanical stress coupling in Piezo actuators and RF coupling in high transmission lines driving for instance high speed integrated optical modulators.

Moreover, an accurate and fast tuning and locking scheme of PICs could be carried on by extracting the exact phase coupling matrix of any arbitrary structure.

There is an Electrical-based measurement method capable of measuring phase coupling matrix. Since conventional PICs benefits from heaters to tune the resonance wavelength of each elements. These heaters are mostly simple resistance fabricated in different platforms i.e. Chromium. The thermal variation (=induced thermal cross-talk) caused by neighboring heaters can be measured in terms of resistance variation.

# Bibliography


[1] G. Cusmai R. Costa A. Breda C. Canavesi A. Melloni, F. Morichetti and M. Martinelli. Progress in large integration scale circuits in sion technology. 1:223–226, 07 2007.

[2] Abdulaziz Al-hetar, Abu Supa'at, Abu bakar Mohammad, and Ian Yulianti. Crosstalk improvement of a thermo-optic polymer waveguide mzimmi switch. 281:5764–5767, 08 2008.

[3] P. Alipour, A. A. Eftekhar, A. H. Atabaki, Q. Li, S. Yegnanarayanan, C. K. Madsen, and A. Adibi. Fully reconfigurable compact rf photonic filters using high-q silicon microdisk resonators. In *2010 23rd Annual Meeting of the IEEE Photonics Society*, pages 236–237, Nov 2010.

[4] A. H. Atabaki, E. Shah Hosseini, A. A. Eftekhar, S. Yegnanarayanan, and A. Adibi. Optimization of metallic microheaters for high-speed reconfigurable silicon photonics. *Opt. Express*, 18(17):18312–18323, Aug 2010.

[5] T. Barwicz, M. A. Popovic, M. R. Watts, P. T. Rakich, E. P. Ippen, and H. I. Smith. Fabrication of add-drop filters based on frequency-matched microring resonators. *Journal of Lightwave Technology*, 24(5):2207–2218, May 2006.

[6] A. Biberman, N. Sherwood-Droz, B. G. Lee, M. Lipson, and K. Bergman. Thermally active 44 non-blocking switch for networks-on-chip. In *LEOS 2008 - 21st Annual Meeting of the IEEE Lasers and Electro-Optics Society*, pages 370–371, Nov 2008.

[7] Krzysztof Borzycki. Labeling of signals in optical networks and its applications.

[8] M. Briere, B. Girodias, Y. Bouchebaba, G. Nicolescu, F. Mieyeville, F. Gaffiot, and I. O'Connor. System level assessment of an optical noc in an mpsoc platform. In *2007 Design, Automation Test in Europe Conference Exhibition*, pages 1–6, April 2007.

[9] F.-L. Chao. Trench structure improvement of thermo-optic. 5:1–5, 08 2007.

[10] Long Chen, Nicolás Sherwood-Droz, and Michal Lipson. Compact bandwidth-tunable microring resonators. *Opt. Lett.*, 32(22):3361–3363, Nov 2007.

[11] C. Condrat, P. Kalla, and S. Blair. Thermal-aware synthesis of integrated photonic ring resonators. In *2014 IEEE/ACM International Conference on Computer-Aided Design (ICCAD)*, pages 557–564, Nov 2014.

[12] C. Condrat, P. Kalla, and S. Blair. Thermal-aware synthesis of integrated photonic ring resonators. In *2014 IEEE/ACM International Conference on Computer-Aided Design (ICCAD)*, pages 557–564, Nov 2014.

[13] Jonathan A. Cox, Anthony L. Lentine, Douglas C. Trotter, and Andrew L. Starbuck. Control of integrated micro-resonator wavelength via balanced homodyne locking. *Opt. Express*, 22(9):11279–11289, May 2014.

[14] Yunhong Ding, Minhao Pu, Liu Liu, Jing Xu, Christophe Peucheret, Xinliang Zhang, Dexiu Huang, and Haiyan Ou. Bandwidth and wavelength-tunable optical bandpass filter based on silicon microring-mzi structure. *Opt. Express*, 19(7):6462–6470, Mar 2011.

[15] Stevan S. Djordjevic, Kuanping Shang, Binbin Guan, Stanley T. S. Cheung, Ling Liao, Juthika Basak, Hai-Feng Liu, and S. J. B. Yoo. Cmos-compatible, athermal silicon ring modulators clad with titanium dioxide. *Opt. Express*, 21(12):13958–13968, Jun 2013.

[16] C. R. Doerr, L. L. Buhl, L. Chen, and N. Dupuis. Monolithic flexible-grid 1 ,*times*,2 wavelength-selective switch in silicon photonics. *Journal of Lightwave Technology*, 30(4):473–478, Feb 2012.

[17] Po Dong, Wei Qian, Hong Liang, Roshanak Shafiiha, Dazeng Feng, Guoliang Li, John E. Cunningham, Ashok V. Krishnamoorthy, and Mehdi Asghari. Thermally tunable silicon racetrack resonators with ultralow tuning power. *Opt. Express*, 18(19):20298–20304, Sep 2010.

[18] R. Enright, S. Lei, K. Nolan, I. Mathews, A. Shen, G. Levaufre, R. Frizzell, G. Duan, and D. Hernon. A vision for thermally integrated photonics systems. *Bell Labs Technical Journal*, 19:31–45, 2014.

[19] R. Enright, S. Lei, K. Nolan, I. Mathews, A. Shen, G. Levaufre, R. Frizzell, G. Duan, and D. Hernon. A vision for thermally integrated photonics systems. *Bell Labs Technical Journal*, 19:31–45, 2014.

[20] Sahba Talebi Fard, Kyle Murray, Michael Caverley, Valentina Donzella, Jonas Flueckiger, Samantha M. Grist, Edgar Huante-Ceron, Shon A. Schmidt, Ezra Kwok, Nicolas A. F. Jaeger, Andrew P. Knights, and Lukas Chrostowski. Silicon-on-insulator sensors using integrated resonance-enhanced defect-mediated photodetectors. *Opt. Express*, 22(23):28517–28529, Nov 2014.

[21] F. Gan, T. Barwicz, M. A. Popovic, M. S. Dahlem, C. W. Holzwarth, P. T. Rakich, H. I. Smith, E. P. Ippen, and F. X. Kartner. Maximizing the thermo-optic tuning range of silicon photonic structures. In *2007 Photonics in Switching*, pages 67–68, Aug 2007.

[22] Minming Geng, Lianxi Jia, Lei Zhang, Lin Yang, Ping Chen, Tong Wang, and Yuliang Liu. Four-channel reconfigurable optical add-drop multiplexer based on photonic wire waveguide. *Opt. Express*, 17(7):5502–5516, Mar 2009.

[23] Minming Geng, Lianxi Jia, Lei Zhang, Lin Yang, Ping Chen, Tong Wang, and Yuliang Liu. Four-channel reconfigurable optical add-drop multiplexer based on photonic wire waveguide. *Opt. Express*, 17(7):5502–5516, Mar 2009.

[24] G. Gilardi, W. Yao, H. Rabbani Haghighi, X. J. M. Leijtens, M. K. Smit, and M. J. Wale. Deep trenches for thermal crosstalk reduction in inp-based photonic integrated circuits. *Journal of Lightwave Technology*, 32(24):4864–4870, Dec 2014.

[25] G. Gilardi, W. Yao, H. Rabbani Haghighi, X. J. M. Leijtens, M. K. Smit, and M. J. Wale. Deep trenches for thermal crosstalk reduction in inp-based photonic integrated circuits. *Journal of Lightwave Technology*, 32(24):4864–4870, Dec 2014.

[26] Giovanni Gilardi and Meint K. Smit. Generic inp-based integration technology: Present and prospects. 46:23–35, 06 2014.

[27] Stefano Grillanda, Marco Carminati, Francesco Morichetti, Pietro Ciccarella, Andrea Annoni, Giorgio Ferrari, Michael Strain, Marc Sorel, Marco Sampietro, and Andrea Melloni. Non-invasive monitoring and control in silicon photonics using cmos integrated electronics. *Optica*, 1(3):129–136, Sep 2014.

[28] Stefano Grillanda, Marco Carminati, Francesco Morichetti, Pietro Ciccarella, Andrea Annoni, Giorgio Ferrari, Michael Strain, Marc Sorel, Marco Sampietro, and Andrea Melloni. Non-invasive monitoring and control in silicon photonics using cmos integrated electronics. *Optica*, 1(3):129–136, Sep 2014.

[29] Biswajeet Guha, Alexander Gondarenko, and Michal Lipson. Minimizing temperature sensitivity of silicon mach-zehnder interferometers. *Opt. Express*, 18(3):1879–1887, Feb 2010.

[30] R. Jones O. Cohen D. Hak R. Nicolaescu A. Fang H. Rong, A. Liu and M. Paniccia. An all-silicon raman laser. pages 292–294, 2005.

[31] Y. H. Kuo V. Sih O. Cohen O. Raday H. Rong, S. Xu and M. Paniccia. Low-threshold continuous-wave raman silicon laser. 1(4):232–237, 2007.

[32] M. Haurylau, G. Chen, H. Chen, J. Zhang, N. A. Nelson, D. H. Albonesi, E. G. Friedman, and P. M. Fauchet. On-chip optical interconnect roadmap: Challenges and critical directions. *IEEE Journal of Selected Topics in Quantum Electronics*, 12(6):1699–1705, Nov 2006.

[33] C.W. Holzwarth, Tymon Barwicz, M.A. Popovic, P.T. Rakich, E.P. Ippen, Franz Krtner, and Henry I. Smith. Accurate resonant frequency spacing of microring filters without postfabrication trimming. 24:3244–3247, 11 2006.

[34] R. Grover J. Heebner and T. Ibrahim. Optical microresonators: Theory, fabrication and applications, 1st edn.

[35] M. A. Foster A. C. Turner-Foster A. L. Gaeta J. S. Levy, A. Gondarenko and M. Lipson. Cmos-compatible multiple-wavelength oscillator for on-chip optical interconnects. 4(1):pages = ,, 2010.

[36] H. Jayatilleka, H. Shoman, R. Boeck, N. A. F. Jaeger, L. Chrostowski, and S. Shekhar. Automatic configuration and wavelength locking of coupled silicon ring resonators. *Journal of Lightwave Technology*, 36(2):210–218, Jan 2018.

[37] Ruiqiang Ji, Lin Yang, Lei Zhang, Yonghui Tian, Jianfeng Ding, Hongtao Chen, Yangyang Lu, Ping Zhou, and Weiwei Zhu. Microring-resonator-based four-port optical router for photonic networks-on-chip. *Opt. Express*, 19(20):18945–18955, Sep 2011.

[38] Sofie Lambert, Wout De Cort, Jeroen Beeckman, Kristiaan Neyts, and Roel Baets. Trimming of silicon-on-insulator ring resonators with a polymerizable liquid crystal cladding. *Opt. Lett.*, 37(9):1475–1477, May 2012.

[39] Jong-Moo Lee and Gyungock Kim. Multichannel silicon wdm ring filters fabricated with duv lithography. 281:4302–4306, 09 2008.

[40] Ming-Chang M. Lee and Ming C. Wu. Variable bandwidth of dynamic add-drop filters based on coupling-controlled microdisk resonators. *Opt. Lett.*, 31(16):2444–2446, Aug 2006.

[41] H. Li, A. Fourmigue, S. Le Beux, I. O'Connor, and G. Nicolescu. Towards maximum energy efficiency in nanophotonic interconnects with thermal-aware on-chip laser tuning. *IEEE Transactions on Emerging Topics in Computing*, 6(3):343–356, July 2018.

[42] Yu Li and Andrew W. Poon. Active resonance wavelength stabilization for silicon microring resonators with an in-resonator defect-state-absorption-based photodetector. *Opt. Express*, 23(1):360–372, Jan 2015.

[43] B.E. Little, J.S. Foresi, Guenter Steinmeyer, E.R. Thoen, Sai Chu, H.A. Haus, E.P. Ippen, L.C. Kimerling, and W Greene. Ultra-compact si-sio2 microring resonator optical channel dropping filters. 10:549 – 551, 05 1998.

[44] J. E. Sharping B. S. Schmidt M. Lipson M. A. Foster, A. C. Turner and A. L. Gaeta. pages 960–963, 2006.

[45] F. Michelotti M. Bertolotti, A. Driessen. Microresonators as building block for vlsi photonics. 2004.

[46] C. K. Madsen. General iir optical filter design for wdm applications using all-pass filters. *Journal of Lightwave Technology*, 18(6):860–868, June 2000.

[47] J. C. C. Mak, W. D. Sacher, T. Xue, J. C. Mikkelsen, Z. Yong, and J. K. S. Poon. Automatic resonance alignment of high-order microring filters. *IEEE Journal of Quantum Electronics*, 51(11):1–11, Nov 2015.

[48] J. C. C. Mak, W. D. Sacher, T. Xue, J. C. Mikkelsen, Z. Yong, and J. K. S. Poon. Automatic resonance alignment of high-order microring filters. *IEEE Journal of Quantum Electronics*, 51(11):1–11, Nov 2015.

[49] J. C. C. Mak, W. D. Sacher, T. Xue, J. C. Mikkelsen, Z. Yong, and J. K. S. Poon. Automatic resonance alignment of high-order microring filters. *IEEE Journal of Quantum Electronics*, 51(11):1–11, Nov 2015.

[50] Sasikanth Manipatruni, Rajeev K. Dokania, Bradley Schmidt, Nicolás Sherwood-Droz, Carl B. Poitras, Alyssa B. Apsel, and Michal Lipson. Wide temperature range operation of micrometer-scale silicon electro-optic modulators. *Opt. Lett.*, 33(19):2185–2187, Oct 2008.

[51] Sasikanth Manipatruni, Rajeev K. Dokania, Bradley Schmidt, Nicolás Sherwood-Droz, Carl B. Poitras, Alyssa B. Apsel, and Michal Lipson. Wide temperature range operation of micrometer-scale silicon electro-optic modulators. *Opt. Lett.*, 33(19):2185–2187, Oct 2008.

[52] A. Melloni and M. Martinelli. Synthesis of direct-coupled-resonators bandpass filters for wdm systems. *Journal of Lightwave Technology*, 20(2):296–303, Feb 2002.

[53] Andrea Melloni and Francesco Morichetti. Tunable photonic circuits: a leap toward system-on-a-chip optical integration. *SPIE Newsroom, Jun*, 2012.

[54] D. A. B. Miller. Device requirements for optical interconnects to silicon chips. *Proceedings of the IEEE*, 97(7):1166–1185, July 2009.

[55] M. Mohamed, Z. Li, X. Chen, L. Shang, and A. R. Mickelson. Reliability-aware design flow for silicon photonics on-chip interconnect. *IEEE Transactions on Very Large Scale Integration (VLSI) Systems*, 22(8):1763–1776, Aug 2014.

[56] F. Morichetti, S. Grillanda, and A. Melloni. Breakthroughs in photonics 2013: Toward feedback-controlled integrated photonics, April 2014.

[57] F. Morichetti, S. Grillanda, and A. Melloni. Breakthroughs in photonics 2013: Toward feedback-controlled integrated photonics. *IEEE Photonics Journal*, 6(2):1–6, April 2014.

[58] P. Orlandi, F. Morichetti, M. J. Strain, M. Sorel, P. Bassi, and A. Melloni. Photonic integrated filter with widely tunable bandwidth. *Journal of Lightwave Technology*, 32(5):897–907, March 2014.

[59] Piero Orlandi, Francesco Morichetti, Michael John Strain, Marc Sorel, Paolo Bassi, and Andrea Melloni. Photonic integrated filter with widely tunable bandwidth. *J. Lightwave Technol.*, 32(5):897–907, Mar 2014.

[60] K. Padmaraju and K. Bergman. Resolving the thermal challenges for silicon microring resonator devices. 2013.

[61] K. Padmaraju, D. F. Logan, T. Shiraishi, J. J. Ackert, A. P. Knights, and K. Bergman. Wavelength locking and thermally stabilizing microring resonators using dithering signals. *Journal of Lightwave Technology*, 32(3):505–512, Feb 2014.

[62] K. Padmaraju, D. F. Logan, T. Shiraishi, J. J. Ackert, A. P. Knights, and K. Bergman. Wavelength locking and thermally stabilizing microring resonators using dithering signals. *Journal of Lightwave Technology*, 32(3):505–512, Feb 2014.

[63] Kishore Padmaraju, Johnnie Chan, Long Chen, Michal Lipson, and Keren Bergman. Thermal stabilization of a microring modulator using feedback control. *Opt. Express*, 20(27):27999–28008, Dec 2012.

[64] Kishore Padmaraju, Johnnie Chan, Long Chen, Michal Lipson, and Keren Bergman. Thermal stabilization of a microring modulator using feedback control. *Opt. Express*, 20(27):27999–28008, Dec 2012.

[65] Kishore Padmaraju, Dylan F. Logan, Xiaoliang Zhu, Jason J. Ackert, Andrew P. Knights, and Keren Bergman. Integrated thermal stabilization of a microring modulator. *Opt. Express*, 21(12):14342–14350, Jun 2013.

[66] Sahnggi Park, Kap-Joong Kim, Jong-Moo Lee, In-Gyoo Kim, and Gyungock Kim. Adjusting resonant wavelengths and spectral shapes of ring resonators using a cladding sin layer or koh solution. *Opt. Express*, 17(14):11884–11891, Jul 2009.

[67] R. Patnaik, V. Vandrasi, C. K. Madsen, A. A. Eftekhar, and A. Adibi. Comparison of cascade, lattice, and parallel filter architectures. *Journal of Lightwave Technology*, 28(23):3463–3469, Dec 2010.

[68] Joyce K. Poon, Lin Zhu, Guy A. DeRose, and Amnon Yariv. Transmission and group delay of microring coupled-resonator optical waveguides. *Opt. Lett.*, 31(4):456–458, Feb 2006.

[69] C. V. Poulton, P. Dong, and Y. Chen. Photoresistive microring heater with resonance control loop. In *2015 Conference on Lasers and Electro-Optics (CLEO)*, pages 1–2, May 2015.

[70] Ashok M. Prabhu, Hai Ling Liew, and Vien Van. Generalized parallel-cascaded microring networks for spectral engineering applications. *J. Opt. Soc. Am. B*, 25(9):1505–1514, Sep 2008.

[71] Joanna N. Ptasinski, Iam-Choon Khoo, and Yeshaiahu Fainman. Passive temperature stabilization of silicon photonic devices using liquid crystals. In *Materials*, 2014.

[72] S. Pradhan Q. Xu, B. Schmidt and M. Lipson. Micrometre-scale silicon electro-optic modulator. 2005.

[73] A. Qouneh, Z. Li, M. Joshi, W. Zhang, X. Fu, and T. Li. Aurora: A thermally resilient photonic network-on-chip architecture. In *2012 IEEE 30th International Conference on Computer Design (ICCD)*, pages 379–386, Sept 2012.

[74] V. Raghunathan Y. Han R. Claps, D. Dimitropoulos and B. Jalali. Observation of stimulated raman amplification in silicon waveguides.

[75] D.G. Rabus. Ring resonators: Theory and modeling. 127:3–40, 01 2007.

[76] Dominik Rabus. *Integrated Ring Resonators The Compendium*, volume 127. 01 2007.

[77] M. S. Rasras, D. M. Gill, S. S. Patel, K. Y. Tu, Y. K. Chen, A. E. White, A. T. S. Pomerene, D. N. Carothers, M. J. Grove, D. K. Sparacin, J. Michel, M. A. Beals, and L. C. Kimerling. Demonstration of a fourth-order pole-zero optical filter integrated using cmos processes. *Journal of Lightwave Technology*, 25(1):87–92, Jan 2007.

[78] H. Shen S. Xiao, M. H. Khan and M. Qi. Multiple-channel silicon micro-resonator based filters for wdm applications. 15(12):7489–7498, 2007.

[79] S. Moro J. M. Chavez Boggio I. B. Divliansky N. Alic S. Mookherjea S. Zlatanovic, J. S. Park and S. Radic. Mid-infrared wavelength conversion in silicon waveguides using ultra compact telecom-band-derived pump source. pages 561–564, 2010.

[80] D. Sadot and E. Boimovich. Tunable optical filters for dense wdm networks. *IEEE Communications Magazine*, 36(12):50–55, Dec 1998.

[81] J. Schrauwen, D. Van Thourhout, and R. Baets. Trimming of silicon ring resonator by electron beam induced compaction and strain. *Opt. Express*, 16(6):3738–3743, Mar 2008.

[82] O. Schwelb. Transmission, group delay, and dispersion in single-ring optical resonators and add/drop filters-a tutorial overview. *Journal of Lightwave Technology*, 22(5):1380–1394, May 2004.

[83] C. T. Shih, Z. W. Zeng, and S. Chao. Extinction ratio compensation by free carrier injection for a mos-capacitor microring optical modulator subjected to temperature drifting. In *2009 Conference on Lasers Electro Optics The Pacific Rim Conference on Lasers and Electro-Optics*, pages 1–2, Aug 2009.

[84] Benjamin A. Small, Benjamin G. Lee, Keren Bergman, Qianfan Xu, and Michal Lipson. Multiple-wavelength integrated photonic networks based on microring resonator devices. *J. Opt. Netw.*, 6(2):112–120, Feb 2007.

[85] C. Sun, C. O. Chen, G. Kurian, L. Wei, J. Miller, A. Agarwal, L. Peh, and V. Stojanovic. Dsent - a tool connecting emerging photonics with electronics for opto-electronic networks-on-chip modeling. In *2012 IEEE/ACM Sixth International Symposium on Networks-on-Chip*, pages 201–210, May 2012.

[86] M. N. Sysak, D. Liang, R. G. Beausoleil, R. Jones, and J. E. Bowers. Thermal management in hybrid silicon lasers. In *2013 Optical Fiber Communication Conference and Exposition and the National Fiber Optic Engineers Conference (OFC/NFOEC)*, pages 1–3, March 2013.

[87] E. Timurdogan, A. Biberman, D. C. Trotter, C. Sun, M. Moresco, V. Stojanovi, and M. R. Watts. Automated wavelength recovery for microring resonators. In *2012 Conference on Lasers and Electro-Optics (CLEO)*, pages 1–2, May 2012.

[88] E. Timurdogan, A. Biberman, D. C. Trotter, C. Sun, M. Moresco, V. Stojanovi, and M. R. Watts. Automated wavelength recovery for microring resonators. In *2012 Conference on Lasers and Electro-Optics (CLEO)*, pages 1–2, May 2012.

[89] Y. A. Vlasov X. Liu, R. M. Osgood Jr and W. M. L. Green. Mid-infrared optical parametric amplifier using silicon nanophotonic waveguides. 4(8),:557–560, 2010.

[90] F. Xia, M. Rooks, L. Sekaric, and Y. Vlasov. Ultra-compact silicon wdm optical filters with flat - top response for on-chip optical interconnects. In *2007 Conference on Lasers and Electro-Optics (CLEO)*, pages 1–2, May 2007.

[91] Fengnian Xia, Mike Rooks, Lidija Sekaric, and Yurii Vlasov. Ultra-compact high order ring resonator filters using submicron silicon photonic wires for on-chip optical interconnects. *Opt. Express*, 15(19):11934–11941, Sep 2007.

[92] Fengnian Xia, Lidija Sekaric, and Yurii Vlasov. Ultracompact optical buffers on a silicon chip. 1:65–71, 12 2006.

[93] Jin Yao and Ming C. Wu. Bandwidth-tunable add–drop filters based on micro-electro-mechanical-system actuated silicon microtoroidal resonators. *Opt. Lett.*, 34(17):2557–2559, Sep 2009.

[94] Y. Ye, Z. Wang, P. Yang, J. Xu, X. Wu, X. Wang, M. Nikdast, Z. Wang, and L. H. K. Duong. System-level modeling and analysis of thermal effects in wdm-based optical networks-on-chip. *IEEE Transactions on Computer-Aided Design of Integrated Circuits and Systems*, 33(11):1718–1731, Nov 2014.

[95] Y. Ye, J. Xu, X. Wu, W. Zhang, X. Wang, M. Nikdast, Z. Wang, and W. Liu. System-level modeling and analysis of thermal effects in optical networks-on-chip. *IEEE Transactions on Very Large Scale Integration (VLSI) Systems*, 21(2):292–305, Feb 2013.

[96] Jong-Bum You, Miran Park, Jeong-Woo Park, and Gyungock Kim. 12.5 gbps optical modulation of silicon racetrack resonator based on carrier-depletion in asymmetric p-n diode. *Opt. Express*, 16(22):18340–18344, Oct 2008.

[97] K. Yu, H. Li, C. Li, A. Titriku, A. Shafik, B. Wang, Z. Wang, R. Bai, C. Chen, M. Fiorentino, P. Y. Chiang, and S. Palermo. 22.4 a 24gb/s 0.71pj/b si-photonic source-synchronous receiver with adaptive equalization and microring wavelength stabilization. In *2015 IEEE International Solid-State Circuits Conference - (ISSCC) Digest of Technical Papers*, pages 1–3, Feb 2015.

[98] Z. Yuan, W. Li, X. Wu, R. Yang, J. Guo, F. Wang, L. Song, Q. Hu, L. Sun, D. Xie, and Z. Xu. Bandwidth and wavelength tunable optical passband filter with tunable attenuation based on transmission liquid crystal technology. In *2017 16th International Conference on Optical Communications and Networks (ICOCN)*, pages 1–3, Aug 2017.

[99] Lei Zhang, Mei Yang, Yingtao Jiang, Emma E. Regentova, and Enyue Lu. Generalized wavelength routed optical micronetwork in network-on-chip. 2006.

[100] Xuezhe Zheng, Eric Chang, Philip Amberg, Ivan Shubin, Jon Lexau, Frankie Liu, Hiren Thacker, Stevan S. Djordjevic, Shiyun Lin, Ying Luo, Jin Yao, Jin-Hyoung Lee, Kannan Raj, Ron Ho, John E. Cunningham, and Ashok V. Krishnamoorthy. A high-speed, tunable silicon photonic ring modulator integrated with ultra-efficient active wavelength control. *Opt. Express*, 22(10):12628–12633, May 2014.

[101] J. Zhou, M. J. O'Mahony, and S. D. Walker. Analysis of optical crosstalk effects in multi-wavelength switched networks. *IEEE Photonics Technology Letters*, 6(2):302–305, Feb 1994.

[102] X. Zhu, K. Padmaraju, L. Luo, M. Glick, R. Dutt, M. Lipson, and K. Bergman. Fast wavelength locking of a microring resonator. In *2014 Optical Interconnects Conference*, pages 11–12, May 2014.

# Acknowledgment

I wholeheartedly thank my advisors Professor A.Melloni, who played a great role in nurturing me over the course of this thesis work.
I gratefully thank M.Milanizadeh for all the great help, the availability and the valuable advice he offered me during this thesis.
I would also like to thank F. Morichetti and the rest of Polifab colleagues who supported me during this work.
Finally, I thank my dear family and my good friend Soha, who never stopped supporting me, no matter how wrong I seemed to be going forward.

As the final word, this research has been given to me as a part of curriculum in 2 years master degree in telecommunication engineering in Politecnico di Milano. I did my best to perform an effective task and hope to relate the work conceivable enough to be comprehended by succeeding readers.